3-21-2005

Deconvolution Analysis of Laser Pulse Profiles from 3-D LADAR Temporal Returns

Michael D. Walter

Deconvolution Analysis of Laser Pulse Profiles From 3-D LADAR Temporal Returns

THESIS

Michael D. Walter, Captain, USAF

AFIT/GE/ENG/05-22

DEPARTMENT OF THE AIR FORCE
AIR UNIVERSITY

AIR FORCE INSTITUTE OF TECHNOLOGY

Wright-Patterson Air Force Base, Ohio

AFIT/GE/ENG/05-22

Deconvolution Analysis of Laser Pulse Profiles From 3-D LADAR Temporal Returns

THESIS

Presented to the Faculty

Department of Electrical and Computer Engineering

Graduate School of Engineering and Management

Air Force Institute of Technology

Air University

Air Education and Training Command

In Partial Fulfillment of the Requirements for the

Degree of Master of Science in Electrical Engineering

Michael D. Walter, B.S.E.E.

Captain, USAF

March 2005

AFIT/GE/ENG/05-22

Deconvolution Analysis of Laser Pulse Profiles From 3-D LADAR Temporal Returns

Michael D. Walter, B.S.E.E.

Captain, USAF

Approved:

/signed/	21 Mar 2005
Dr. Stephen Cain (Chairman)	date
/signed/	21 Mar 2005
Dr. Robert F. Mills (Member)	date
/signed/	21 Mar 2005
Dr. Michael A. Temple (Member)	date

AFIT/GE/ENG/05-22

Abstract

3-D laser imaging systems offer important advantages for battle field applications such as night-time targeting and tactical reconnaissance. Recently developed technologies used by coherent detection systems that collect temporally resolved images include arrays of Avalanche Photo-Diodes (APD), Geiger mode APDs', and photo-diodes. Frequently, LADAR systems produce waveforms from each detector that characterize the convolution of the transmitted laser pulse with the target surface. The pulse convolution generates uncertainty as to the precise location of a target surface which can severely impact various weapons systems' targeting capability.

This work analyzes two deconvolution techniques: Wiener filtering and an iterative process derived from negative binomial statistics. Measured and simulated data are used for testing both methods. 3-D imaging LADAR systems with rapid frame acquisition may lose range resolution due to the transmitted pulse duration. Because of the tradeoff between the need for sufficient target illumination and obtaining high range resolution, LADAR systems often forfeit range resolution performance to improve the signal-to-noise ratio of the observed signal. This work also utilizes these two deconvolution techniques on a sequence of LADAR return images gathered at a very high sampling rate to improve the system's range resolution. Deconvolving the data amplifies any noise present in the data and decreases the signal-to-noise ratio of the reconstructed return pulse profiles.

Based on the presence of photon and speckle noise, the work explores the degree to which range resolution can be improved for both measured and simulated data. Squared error and variance calculations are used to evaluate the performance of both signal reconstruction algorithms. The work shows that applying the iterative algorithm to measured and simulated data significantly improves the data's temporal resolution compared to the Wiener filter results.

Acknowledgements

First and foremost, I would like to express my sincere appeciation to my thesis advisor, Dr. Stephen Cain, for his guidance and support throughout the course of this thesis effort. The insight and background he provided was certainly appreciated. I would also like to thank my sponsors from the Air Force Research Laboratory Sensors Directorate, AFRL/SNJM, for both the support and latitude provided to me in this endeavor. In addition, I would like to thank Dr. Robert Mills and Dr. Michael Temple, for their time, effort, and willingness to be a part of my thesis committee. Special thanks go to my mother, father, and sister for their constant encouragement and support through all phases of this research product.

Michael D. Walter

Table of Contents

List of Figures

List of Tables

Table Page

Deconvolution Analysis of Laser Pulse Profiles From 3-D LADAR Temporal Returns

I. Introduction

The use of three-dimensional laser imaging systems in battlefield operations is one of the most impelling and progressive areas of electro-optical research due to the field's many difficult, yet intriguing, problems. Today, many two-dimensional (2-D) and three-dimensional (3-D) laser imaging systems used for military applications incorporate temporal averaging to enhance images.

Temporal averaging, low pass filtering, is the process of modifying a signal or sequence of images given the presence of noise [1]. It is a form of filtering used to remove excess noise and extraneous information from a signal. If a sequence of images are obtained of a stationary object, the differences between the images are caused by image noise. Image noise is reduced by averaging the images. One pitfall of temporal averaging is the loss of temporal resolution in the data, thereby decreasing the information available to the user regarding range resolution and target position. In addition, temporal averaging creates an added element in the form of motion blur in the system response of the imaging system. Often, these blurring effects can be overcome through various types of image reconstruction techniques. However, resolving 2-D data temporally is a difficult task because little temporal information is available in 2-D data.

Ideally, keeping 3-D laser pulse return data intact gives a laser detection and ranging (LADAR) operator the ability to perform image processing and target detection techniques on the temporal information. Using temporal information will help an operator locate target edges and edges of other objects in the image data.

II. Literature Review

Recent applications of 3-D laser systems in military environments have provided significant advantages in such areas as night targeting, partially obstructed targeting, and tactical reconnaissance [7]. Detecting partially obstructed targets is one particularly difficult problem for targeting systems in military environments. Typical target obstructions in a battlefield environment include camouflage netting, smoke, fog, and foliage.

Emerging new technologies for gathering range resolved images used in coherent 3-D laser image detection systems include Avalanche Photo-Diode (APD) arrays, Geiger mode APD arrays, and photo-diode arrays. Such technologies can aid in the detection of partially obscured targets. The detectors in many of these systems produce waveforms that represent the convolution of the transmitted laser pulse with the target surface. However, the convolution of the pulse creates ambiguity as to the precise location of the surface [2]. The ambiguity severely impacts a LADAR weapon system's precision in detecting targets. Three dimensional LADAR imaging systems capable of rapid frame acquisition may suffer losses in range resolution resulting from the duration of the pulse transmitted to the target. Tradeoffs exist between sufficiently illuminating the target and obtaining higher range resolution, therefore LADAR systems may sacrifice range resolution in favor of improving the signal-to-noise ratio of the detected signal.

2.1 Background

A current imaging processing problem is finding a deconvolution technique that obtains better range resolved LADAR return images collected at very high speeds. Since LADAR data processing must account for unwanted parameters that degrade information contained in the received signal (i.e., temporal resolution), estimation theory can be used to find estimators that accurately represent the original scene.

This thesis presents two deconvolution techniques to improve the temporal resolution of LADAR pulse profile returns in the presence of photon and speckle noise. The first method uses an updating (iterative) deconvolution algorithm that improves the temporal resolution of LADAR pulse profile

returns to locate target surfaces in the presence of photon and speckle noise. The second, common image processing technique, considered uses Wiener filtering to suppress image degrading effects caused by photon and speckle noise. The thesis research analyzes and compares the accuracy and performance of image estimators generated by these two deconvolution techniques using both simulated and real world LADAR data. The performance and accuracy of the estimators generated by both techniques are quantified by comparing the squared error difference values between the true image, the convolved image and the corresponding estimated image. The performance comparison of the deconvolution techniques yield at least two important research contributions. First, previous works in the laser image processing field discuss 3-D deconvolution techniques to improve temporal resolution, but none of these works discuss the application of the iterative algorithm on measured LADAR data and simulated data modeled after the measured data [2, 4, 7]. Second, none of these works compare the performance of the LADAR iterative algorithm with methods typically used in other image processing applications such as Wiener filtering.

2.2 Image Reconstruction Techniques

To solve the above problem, one must understand the process of deconvolving LADAR returns. This section discusses the importance of using deconvolution on LADAR return data. The derivation of a common deconvolution technique, the Richardson-Lucy algorithm, is discussed. Since the iterative algorithm uses premises taken from Richardson-Lucy, the last part of the section examines the background behind his deconvolution technique.

2.2.1 Deconvolution. The primary function of LADAR range finders is producing spatially resolved data measurements [4]. By measuring the time of flight of photons traveling in the LADAR pulse, a relationship between space and time is used to calculate the distance between the system and the target of interest. Accordingly, if the response function of the system is longer than the time resolution of the detector array, the return signal measured by the system will smear. As a result, the system's range resolution capability decreases. By deconvolving the measured return signal with

the system response function, the system corrects the resolution loss. Unfortunately, noise effects are always present in real world LADAR signals. Additive noise makes direct deconvolution impractical due to the amplification of the noise component in the signal. Based on this presence of noise in the LADAR signal, Harsdorf considers conventional deconvolution using pre-filtering and Fourier transforms, as well as the Richardson-Lucy algorithm, to improve the range resolution of LADAR systems.

For the conventional deconvolution analysis, Harsdorf considers a LADAR signal $P_m(t)$ for a single target overlayed with noise. The signal is described by the convolution equation

$$P_m(t) = \int_{-\infty}^{\infty} R(t'-t) * P_\delta(t')dt' + N(t) = [R(t) \otimes P_\delta(t)] + N(t), \tag{2.1}$$

where R(t) is the system response function, $P_\delta(t)$ is the impulse response function of the environment in which the system operates, N(t) is a additive white Gaussian distributed noise signal, and $\otimes$ denotes the convolution. The LADAR signal $P_m(t)$ equals the convolution of R(t) with the impulse response function with noise added. The term convolution is defined as an integral that represents the amount of overlap of one function over another [9]. Performing deconvolution on the convolved signal, reverses this overlapping of the two functions. Since the LADAR signal has an added noise component, performing a direct deconvolution of the signal is unrealizable [4].

2.2.2 Richardson-Lucy Algorithm. The Richardson-Lucy algorithm is a repetitive process developed by W.H Richardson and L.B. Lucy to improve image restoration performance assuming a Poisson distribution [4]. The algorithm assumes the return signal is an image with dimension 1 x N. Based on this assumption, the algorithm can be used to deconvolve signals. The equation for the j-th repetition is

$$P_\delta^{j+1}(t) = P_\delta^j(t)R^T(t) \otimes \frac{P_m(t)}{P_m^j(t)}, \tag{2.2}$$

where

$$P_m^j(t) = R(t) \otimes P_\delta^j(t), \tag{2.3}$$

and $R^T(t)$ is the transpose of the system response function. Both the conventional deconvolution and Richardson-Lucy algorithm provide range resolution improvements. Conventional deconvolution requires a pre-filtering application to remove noise amplification at higher frequencies. Harsdorf claims the Richardson-Lucy algorithm preforms better than the conventional method because the signal output using Richardson-Lucy remains unchanged regardless of the pre-filter application. Since noise is not amplified during the Richardson-Lucy algorithm, the output is independent of any pre-filtering processing applied to the noisy signal.

2.2.3 LADAR Iterative Deconvolution Algorithm. The Richardson-Lucy algorithm is the basis for the development of this iterative deconvolution method. A derivation of the *a posteriori* probability density function, $o(x, y, k_2)$, given the observed waveform, is required to build the iterative algorithm [2]. A Bayesian estimator is calculated by creating the likelihood function conditioned on the data and then maximizing the result with respect to the noted parameters [8]. The likelihood function is built as the conditional *a posteriori* density, or the conditional probability of the parameters, given the recorded image [2].

The relationship between the *a posteriori* density and *a priori* density function via Bayes rule is

$$f_{O|D}(o|d) = \frac{f_{D|O}(d|o)}{f_D(d)}, \tag{2.4}$$

where the *a posteriori* density $f_{O|D}(o|d)$ is the probability of scene o conditioned on the recorded image d. The *a priori* distribution of the data given the scene is

$$f_{D|O}(d|o) = \mathbf{P}(\mathbf{D} = \mathbf{d}|\mathbf{O} = \mathbf{o})$$

.

The parameter d represents a realization of the noisy data, and o is the scene, which is a non-random parameter. The operator $\mathbf{P}$ represents the probability that the image data is equal to a realization of that process conditioned on a scene $O = o$. For each point in the recorded data, this

density is

$$\mathbf{P}[\mathbf{D}(\mathbf{x},\mathbf{y},\mathbf{k}) = \mathbf{d}(\mathbf{x},\mathbf{y},\mathbf{k})|\mathbf{O}(\mathbf{x},\mathbf{y},\mathbf{k_2}) = \mathbf{o}(\mathbf{x},\mathbf{y},\mathbf{k_2})] = \tag{2.5}$$
$$\frac{[d(x,y,k)+M_t]!}{[d(x,y,k)+1]!M_t!}[1+M_t/i(x,y,k)]^{-d(x,y,k)}[1+i(x,y,k)/M_t]^{-M_t}.$$

In the above equation, $i(x,y,k) = \sum_{k_2=1}^{K} h(k-k_2)o(x,y,k_2)$, $h(n)$ represents the convolution of the impulse response of the detector and the laser pulse, and M_t is the speckle parameter [3]. Assuming statistical independence between samples in time results in the probability that a set of random variables $D(x,y,k) = d(x,y,k)$ is

$$\mathbf{P}[\mathbf{D}(\mathbf{x},\mathbf{y},\mathbf{k}) = \mathbf{d}(\mathbf{x},\mathbf{y},\mathbf{k})|\mathbf{O}(\mathbf{x},\mathbf{y},\mathbf{k_2}) = \tag{2.6}$$
$$o(x,y,k_2)\forall(k,k_2) \in (1,2,...,K)] =$$
$$\prod_{k=1}^{K} \frac{[d(x,y,k)+M_t]!}{[d(x,y,k)+1]!M_t!}[1+\frac{M_t}{i(x,y,k)}]^{-d(x,y,k)}[1+\frac{i(x,y,k)}{M_t}]^{-M_t}.$$

The probability density function $f_D(d)$ in the above equation is the probability of the measured image equaling a particular realization of that process unconditioned on any other event. $f_D(d)$ is not a function of the parameters $o(x,y,k_2)$.

By maximizing the *a posteriori* density, or likelihood, an estimator for $o(x,y,k_2)$ is obtained. To simplify the estimator's form, the natural logarithm of the likelihood function is maximized,

$$L(o) = \ln[f_{D|O}(d|o)] - \ln[f_D(d)]. \tag{2.7}$$

This function can be reduced to a function of terms that only depend on the image as given

by

$$L(o) = \ln[f_{D|O}(d|o)]. \tag{2.8}$$

Using the expression for the conditional *a priori* density function from Eqn. 2.7, the log-likelihood becomes

$$L(o) = \sum_{k=1}^{K} \ln[\frac{(d(x,y,k)+M_t)!}{(d(x,y,k)+1)!M_t}] - d(x,y,k)\ln[1+\frac{M_t}{i(x,y,k)}] - M_t \ln[1+\frac{i(x,y,k)}{M_t}]. \tag{2.9}$$

The log-likelihood is differentiated with respect to $o(x,y,k_2)$ and set equal to zero to form a proper estimation of the scene $o(x,y,k_2)$. Before differentiating, the function is simplified by only considering those terms which are dependent on the parameters of interest. The function is simplified further by factoring $i(x,y,k)$ out of the denominator in the second term and M_t out of the denominator in the third term. The resulting function is written as

$$L(o) = \sum_{k=1}^{K} -d(x,y,k)\ln[\frac{i(x,y,k)+M_t}{i(x,y,k)}] - M_t \ln[\frac{M_t+i(x,y,k)}{M_t}]. \tag{2.10}$$

By factoring out the terms in the denominator of the natural logarithms as the negative of their reciprocals and again only keeping terms that are dependent on the parameters of interest, the log-likelihood is expressed as

$$L(o) = \sum_{k=1}^{K} d(x,y,k)\ln[i(x,y,k)] - [d(x,y,k)+M_t]\ln[i(x,y,k)+M_t]. \tag{2.11}$$

Differentiating with respect to $o(x,y,k_2)$ and setting the result equal to zero yields

$$0 = \sum_{k=1}^{K} \frac{d(x,y,k)}{i(x,y,k)}\frac{\delta i(x,y,k)}{\delta o(x,y,k_2)} - \frac{(d(x,y,k)+M_t)}{(i(x,y,k)+M_t)}\frac{\delta i(x,y,k)}{\delta o(x,y,k_2)}. \tag{2.12}$$

Using the relationship $i(x,y,k) = \sum_{n=1}^{K} h(k-k_2)o(x,y,k_2)$ the derivative becomes

$$\frac{\delta i(x,y,k)}{\delta o(x,y,k_2)} = h(k-k_2). \tag{2.13}$$

Substituting the result into the differentiated log-likelihood yields a condition for a maximizer of $L(o)$ with respect to $o(x,y,k_2)$

$$0 = \sum_{k=1}^{K} \frac{d(x,y,k)h(k-k_2)}{i(x,y,k)} - \frac{(d(x,y,k)+M_t)h(k-k_2)}{(i(x,y,k)+M_t)}. \tag{2.14}$$

As M_t becomes large, the second term minimizes to the point spread function, which is comparable with results obtained using a Poisson density instead of a negative-binomial density [2,6]. Similar to the derivation of the Richardson-Lucy algorithm, the negative term is brought over to the left side and both sides are divided by the left side producing

$$1 = \frac{\sum_{k=1}^{K} \frac{d(x,y,k)h(k-k_2)}{i(x,y,m}}{\sum_{k=1}^{K} \frac{(d(x,y,k)+M_t)h(k-k_2)}{(i(x,y,k)+M_t)}}. \tag{2.15}$$

Multiplying both sides by $o(x,y,k_2)$ provides the iterative equation

$$o^{new}(x,y,k_2) = o^{old}(x,y,k_2)\frac{\sum_{k=1}^{K} \frac{d(x,y,k)h(k-k_2)}{i^{old}(x,y,k}}{\sum_{k=1}^{K} \frac{(d(x,y,k)+M_t)h(k-k_2)}{(i^{old}(x,y,k)+M_t)}}. \tag{2.16}$$

In Eqn. 2.16, terms relying on the image estimation from the previous calculation are labeled as old, while the new estimate is on the left-hand side.

2.2.4 Wiener Filtering. An alternate filtering technique, Wiener filtering, uses prior statistical knowledge of the noise to minimize noise effects on the signal [1]. Wiener filtering in the temporal direction is another deconvolution technique used to improve the range resolution of pulse profiles. A Wiener filter is a linear filter constructed to minimize the mean square error (MSE)

between the image on the detector array and some desired image. The filter, in this case, is designed to minimize the MSE between the original convolved pulse profile and the desired pulse profile [1].

A common pre-processing technique performed on the non-zero mean data before filtering is subtracting the mean value from the data set [5]. This aids in removing any bias from the data before filtering. After the data is filtered, the data's mean value is added to the data set. Previous research efforts show that applying the Wiener filter on convolved return pulses reduces noise effects observed in the pre-filtered pulses [4]. The Wiener filter equation is

$$\frac{H^*(u,v)}{|H(u,v)|^2 + \frac{P_n(u,v)}{P_s(u,v)}},$$

where $H(u,v)$ is the Fourier transform of the point spread function, $P_n(u,v)$ is the power spectrum of signal, and $P_n(u,v)$ is the power spectrum of the signal noise. P_n/P_s is constant and for all u,v and can be viewed as the reciprocal of the signal-to-noise ratio [5]. Wiener filters are similar to inverse filters except Wiener filters have an additional noise-to-signal ratio constant that compensates for noise amplification. Varying the value of this constant significantly impacts the deconvolved Wiener filter pulse profile.

III. Solution Methodology

The thesis research focuses on applying the iterative deconvolution and Wiener filtering methods on both simulated and measured LADAR temporal returns. Application of both techniques on different data sets will generate estimators of the true scene. Comparing the squared error difference between the estimator and the true scene for both methods quantifies which method performs better in resolving LADAR temporal returns.

3.1 Scope

The research goal is to apply the iterative deconvolution algorithm and Wiener filtering on different temporal vectors within the noisy data sets. Both techniques generate an estimated vector corresponding to the true scene. Analysis of both methods on the measured data and simulated data includes setting the speckle noise parameter value, M_t, to two different values. The two values used for this research are M_t equal to one and 100, respectively. Since measured data was limited and AFRL has the flexibilty to change the speckle parameter, using these two M_t value extremes on simulated show how the amount of speckle in a LADAR image will effect the performance of the two deconvolution methods. The speckle parameter represents the degree of speckle averaging in the signal due to the coherence of the laser compared to the length of the illumination pulse [2]. M_t equal to 100 represents a LADAR system that has a sampling time much greater than the coherence time of the laser which translates to temporal data that is partially coherent. In addition, the temporal data has a relatively high signal to noise ratio (SNR). The lowest possible value for the speckle parameter M_t equal to one is the most challenging noise environment possible for LADAR data.

Another parameter of interest in researching the two deconvolution methods is the amount of energy in the return data collected by the LADAR system. One way of measuring the light level of the data returns is by counting the number of photons collected by the detector array of LADAR system. Since the LADAR system uses a particular light level to collect the measured data sets, the light level parameter for these data sets is fixed. However, the light level parameter can be adjusted when analyzing the simulated data. Therefore, simulated data analysis includes looking at data

returns with high and low light levels. High light level data will be defined as return data vectors containing approximately 10,000 photons. Low light level data will be defined as return data vectors containing approximately 1,000 photons.

3.2 Assumptions

The research makes several assumptions when determining the form of the estimated image derived from the iterative deconvolution algorithm. These assumptions are also important for evaluating the algorithm's accuracy and performance in estimating the true image.

First, the combined statistics of the speckle and photon noise are assumed to be a negative binomial distribution. Second, the research does not use a definitive detector noise model because this type of noise is dependent upon the specific type of detector used by the LADAR system.

3.3 Metrics

Calculating the squared error difference and the variance between the true scene, the convolved scene, and the estimated scene for the real and simulated data, respectively, will be the primary primary metric used for this research. The squared error and mean squared error calculations are used to compare and contrast the research results of both deconvolution techniques.

3.4 Data

In early October, 2004, AFRL/SNJM recorded LADAR data to be used for researching methods for improving data temporal resolution. An improvement in temporal resolution would help in detected target surfaces and their locations within the given data set. The LADAR system's target of interest for the experiment was a hollow rectangular shaped box with front and back surfaces constructed with plywood. Approximately two dozen square and rectangular shaped holes were cut out of the front surface allowing light to illuminate the inside of the back surface of the target. These cut outs on the front surface made the target symmetrically identical from top to bottom. The target

was positioned such that the front and back surfaces formed a right angle with the LADAR system. Unfortunately, AFRL could not provide the original schematics for the target. Since knowing the target's dimensions were necessary for modeling the simulated data, the researcher coordinated with AFRL/SNJM to measure the target's dimensions.

The parameters for LADAR system and the environment in which the data was measured are listed in Table 3.1. Some parameters (M_t, pulse width, pulse shape) listed in Table 1 are unknown. As a result, these parameters have been estimated based on observations of the measured data in MATLAB®.

3.5 Measured Data

Measured data for the research was recorded, formatted, and provided by the offices of AFRL/SNJM. AFRL recorded both 8-bit and 16-bit signed data, but only the higher resolution 16-bit data was used for the temporal deconvolution analysis. Eleven 16-bit data sets were provided by AFRL for the research effort. AFRL pre-processed the raw data for proper formatting before deconvolution analysis. The last data formatting procedure converted the data into .MAT format since MATLAB® was used for data analysis. Each set of the processed measured data used for the research is 128 pixels square with 21 separate frames (images) profiling the target in the temporal direction.

After visually inspecting each of the 11 data sets, frame-by-frame, only one data set was deemed acceptable for temporal deconvolution analysis. Ideally, each data set should show a gradual transition, frame by frame, from illumination of the target's front surface to illumination of only the cut out sections. The other data sets were unacceptable because the LADAR system's detector aperture closed before receiving the entire return pulse from the target. For example, the one data set labeled showed a transition, frame by frame, from illumination of the target's front surface to illumination of both surfaces. The data set did not contain frames showing illumination of the cut out sections only. As a result, this particular data set cannot be temporally resolved because the LADAR system did not receive the complete pulse return from the target. Unfortunately, with only one measured

data set available an extensive deconvolution analysis of the measured data is limited.

However, the good data set does require additional pre-processing before deconvolution to better resolve the temporal information. Frames 1, 17, and 18 of the data set were corrupted. These frames were removed from the data before deconvolution to avoid additional biasing that would effect the temporally resolved data. In addition, all zero valued pixels are replaced with near zero equivalent positive values to avoid dividing by zero during deconvolution. Removing bad data frames from the data set avoids some biasing, but unknown biases due to the atmosphere, the LADAR system, etc., still may be present in the data. This bias is reduced by taking the data vector of interest and subtracting off the minimum number of photons present in the given data vector. With bias effects reduced due to the data pre-processing, the data set is ready for deconvolution. A relatively large amount of speckle averaging occurs in the return pulse captured by the detector array of the LADAR system, therefore, the speckle averaging parameter for the measured data is assumed to be $M_t = 100$. Figure 3.1 and Figure 3.2 show the data set frame by frame of the measured data set used in the deconvolution analysis. Based on the system sample rate and distance between the target's front and back surfaces, the frame seperation distance of the target's surfaces in the data set are 3 or 4 frames. The front and back surfaces of the target in the measured data set are assumed to be located in the the 6th and 10th frames, respectively.

3.6 Simulated Data

The simulated LADAR data is modeled in the form and characteristics of the real world LADAR data. To accurately model the simulated data, the target's dimensions were measured. A simple ratio using the focal length, pixel pitch, and target distance yields the target length per pixel in the data set. Each pixel in a given image frame of measured data corresponds to 6.92 cm of length in the real world. With this length to pixel conversion, the simulated target was constructed using MATLAB® and positioned in each simulated data set at the same location coordinates as the target in the measured data. Similar to the measured data, each simulated data set has a frame size of

128 pixels squared with 18 separate frames (images) profiling the target in the temporal direction. Figure 3.3 and Figure 3.4 show the front and back target surfaces, including dimensions. The white areas in the figures represent the surfaces of the target as seen from the LADAR system. These surfaces were used to generate the target in the simulated data sets. The front and back surfaces of the target were placed in the 6th and 10th frames of the simulated data set, respectively.

Two parameters of interest in the simulated data research include varying light levels and varying the speckle noise parameter, M_t. These parameters will affect the performance of the iterative and Wiener filter deconvolution methods. The light level and M_t for the measured data are assumed to be fixed, but the exact values are unknown. By varying the light level and M_t, four different scenarios can be analyzed. The four scenarios include high light level and high M_t, low light level and high M_t, high light level and low M_t, and low light level and low M_t. High light level simulated data, based on the number of photons observed in measured data target vectors (between 9000-13000 photons/vector), will have data vectors containing approximately 10000 photons each. Low light level simulated data will have data vectors containing 1000 photons each. As previously discussed, the low M_t value is 1 and the high M_t value is 100.

In order to accurately model the simulated data after the measured data, several convolutions are performed on the pristine simulated data. Also, noise effects must be added. The simulated LADAR pulse must be convolved with the data to simulate the transmitted pulse reflecting off the target. In addition, a combined optical transfer function (OTF), based on the physical properties of the system and the atmosphere, is convolved with the data to simulate the optical and atmospheric effects of the system on the transmitted pulse. Simulated noise effects (photon and speckle) are added to the convolved simulated data. Since photon and speckle noise has a negative binomial distribution, many statistically independent simulated data sets can be generated. As a result, a statistical analysis (variance calculations) of both deconvolution methods can be done [2]. Creating the simulated noise and applying it to the entire data set are extremely time intensive in $MATLAB^{®}$.

Since the target occupies a significantly smaller area than the entire data set, a section of the data set containing the target was cropped for analyzing the two deconvolution methods.

Table 3.1: Measured and Simulated LADAR Data Parameters.

Variable	Value(s)
M_t (measured data)	100 (estimated from detector pixel size)
M_t (simulated data)	1 and 100
Pulse shape	Gaussian (estimated)
λ_{Laser} (wavelength)	1.55e-6 m
Pixel pitch	1.00e-4 m
Number of photons in high light environment (simulated)	10000 photons
Number of photons in low light environment (simulated)	1000 photons
Frame sample rate	2.38e-9 s
Number of uncorrupted frames	18 frames/data set
Number of detectors (square array)	128
Iteration number (iterative algorithm)	10000

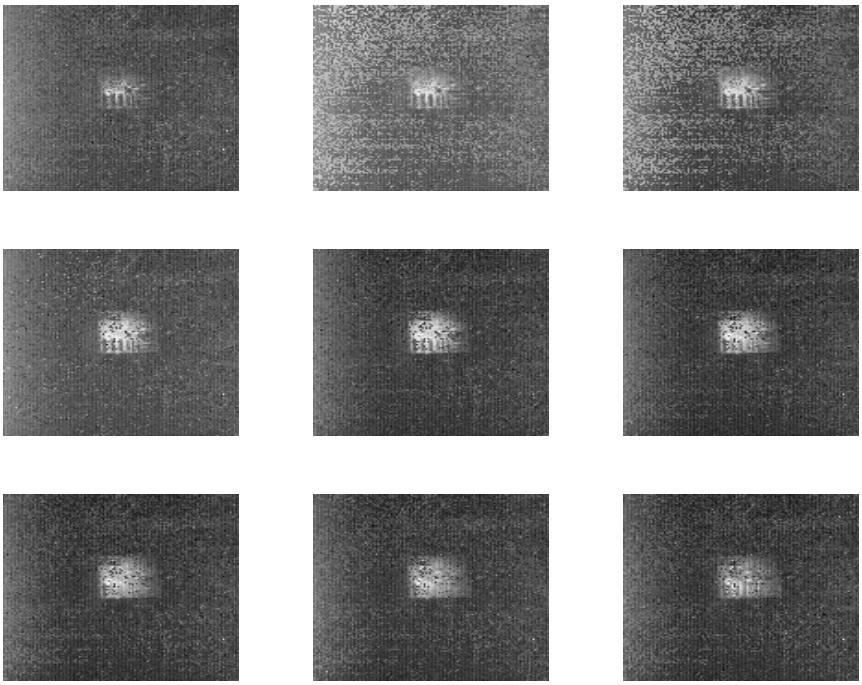

Figure 3.1: First nine frames of the measured data set used for the research.

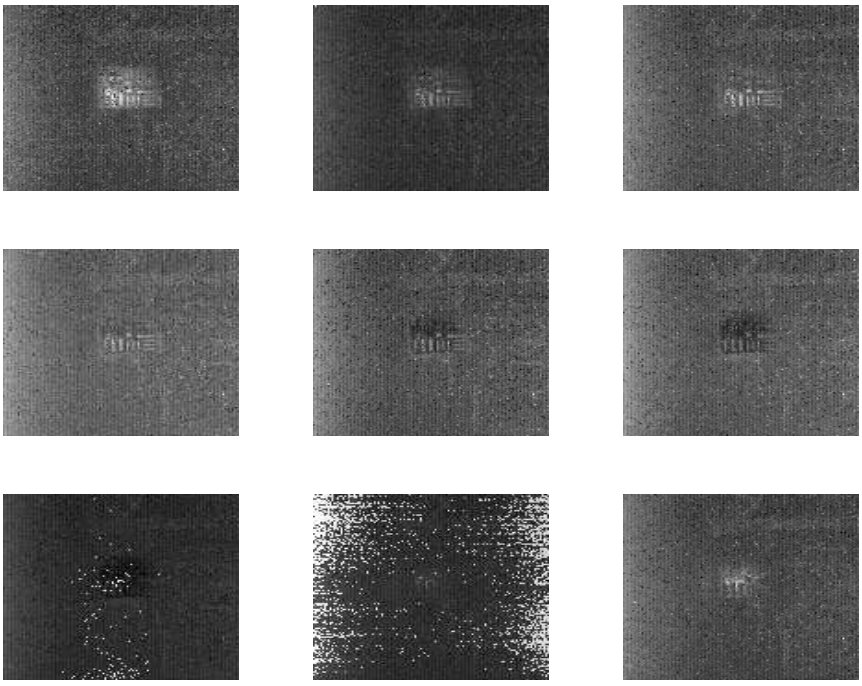

Figure 3.2: Last nine frames of the measured data set used for the research. The simulated data was modeled after all 18 frames of this specific measured data set.

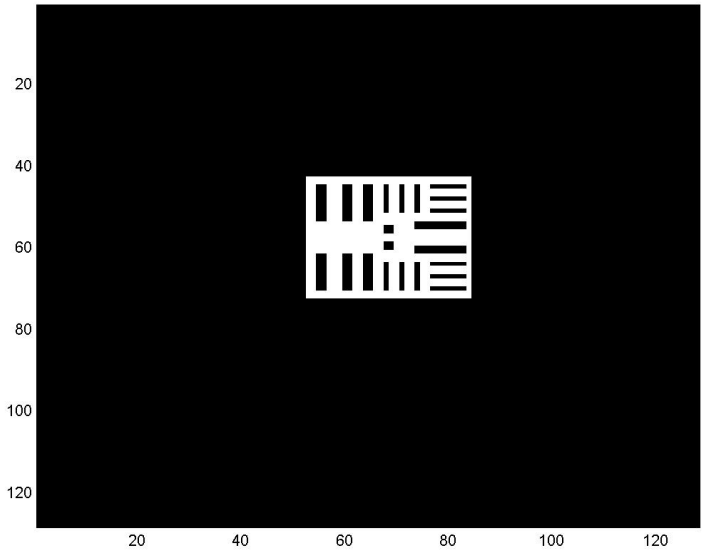

Figure 3.3: The front surface of the target used in the simulated data.

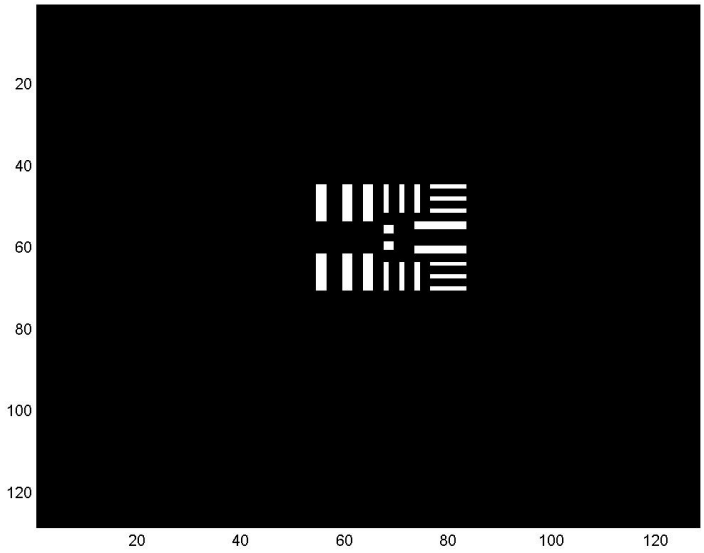

Figure 3.4: The back surface of the target used in the simulated data.

IV. Results for Measured and Simulated Data

The results and discussion of the research are divided into several different categories based on the two data types tested, measured, and simulated. Test results using measured data include deconvolution profiles of the target's front surface and back surface based on the parameters listed in Table 1. Counting the number of photons in data containing the target's front and back surfaces show total photon quantities ranging between 9000 and 13000 photons. Based on these photon quantities, the light level for the measured data is assumed high. The simulated data results include the same deconvolved front and back surface profiles of the target. However, the simulated deconvolution results consider variations in speckle noise parameter values. The simulated data results also show the effect of the LADAR system operating in high and low light level environments.

4.1 Measured Data Results

The measured data test results demonstrate the iterative deconvolution algorithm does a better job temporally resolving the target than the Wiener filter deconvolution. Figure 4.1 represents the convolution of the pulse with the front surface of the target. The convolved data was pre-processed as described in Chapter III. The signal to noise ratio (SNR) of the data appears to be high, based on the shape of the convolved profile. One could make an educated guess as to the location of the target surface based on the peak value of the number of photons. The peak photon quantity will not necessarily correspond to the surface location because the convolution operation most likely causes a left or right shift of the target's true surface location.

The Wiener filtered deconvolution of the target's front surface is shown in Figure 4.2. According to the results in Figure 4.2, the Wiener filtered deconvolved solution has negative photon values. The negative photon values are based on the shape of the convolved data and the functionality of the Wiener filter. Wiener filters are unable to reconstruct features that have been degraded by noise. They can only suppress the noise. Also, Wiener filters are unable to restore components for which the point spread function (PSF) equals zero. The PSF for the purposes of this research is the Fourier Transform of the Gaussian-shaped LADAR pulse. This means Wiener filters are unable to

undo blurring caused by bandlimiting of the PSF. This type of bandlimiting occurs in any real-world imaging system. The Wiener filter is a linear filter, so applying the filter to the convolved data will smooth any sharpness present in the data.

Since the convolved data has a sinusoidal shape, wiener filtering the data will enhance the separation of the the highest and lowest values present. Therefore, straight deconvolution with a Wiener filter may change the lowest values of the data set into negative results. Replacing all negative values in the deconvolved data with zeros and properly scaling the data yields a more accurate representation. After removing the negative values in the filtered data, scaling the data was accomplished by keeping the total number of photons consistent between the convolved and deconvolved data. Figure 4.3 displays the non-negative, properly scaled, Wiener filter deconvolved solution for the target's front surface location. Based on the location of the maximum number of photons in Figure 4.3, the target's front surface is located in the 6th frame of the data set.

The final iteration of the deconvolved data is plotted in Figure 4.4. The iterative algorithm equation begins with $o(x, y, k_2) = 1$ and is found to converge after at least one thousand iterations. For the purposes of this research, the iteration number is 10000 for all iterative algorithm test results. These additional iterations add robustness to the final iterative solution. All 10000 iterations of the deconvolved data are shown in Figure 4.5. Based on the iterative algorithm results, the target's front surface location is in 6th frame of the data set.

Both deconvolution methods yield the same target surface location, frame six, in the data set. However, the squared error difference between the deconvolved profiles from both methods and the true location of the surface show that the iterative algorithm generates a much better estimation of the target's front surface. Figure 4.6 shows that the squared error values for the deconvolved profile from the Wiener filter and the convolved profile are very similar. The three squared error (SE) values are calculated using the different pulse profiles and target's front surface location in the true scene. The maximum squared error values for the three different pulse profiles illustrate how well the iterative algorithm performs over the Wiener filter. The Wiener filter's maximum squared error

value is approximately 29.3 times larger than the maximum squared error of the iterative algorithm.

Similar deconvolution results were found with containing the target's back surface. Figure 4.7 represents the convolution of the pulse with the back surface of the target. The true Wiener filter deconvolved profile as discussed above is given in Figure 4.8. Based on the Wiener filter results, the target's back surface location is approximately the 11th frame of the data set.

The 10000th iteration of the data for find the target's back surface is plotted in Figure 4.9. Similar to the results for finding the front surface, the iterative algorithm is found to converge after at least one thousand iterations. All 10000 iterations of the deconvolved data are shown in Figure 4.10. Based on the iterative algorithm results, the target's back surface is in the 10th frame of the data set.

Both deconvolution methods provide approximately the same estimation for the target's back surface. However, the square error difference between the deconvolved profiles from both methods and the true location of the surface shows that the iterative algorithm generates a much better estimation of the target's back surface. The squared error calculations for both deconvolution methods are given in Figure 4.11. The maximum squared error values for both methods illustrate how much better the iterative algorithm performs over the Wiener filter. The Wiener filtered profile shows virtually no improvement in temporal resolution compared to the convolved profile. The Wiener filter's maximum squared error value is approximately 8.4 times larger than the maximum squared error of the iterative algorithm. The discrepancy between the different frame locations given by the two methods is solved by examining the squared error results. Since the iterative algorithm solution has a smaller squared error, the target's back surface is located in the 10th frame of the data set.

4.2 Simulated Data Results

The simulated data including the target was modeled after the data used in the measured data tests. Based on the deconvolved measured data, the target's front and back surfaces were placed in the 6th and 10th frames, respectively, of each simulated data set. Changing the level light and

M_t values do effect the performance of both methods but the iterative method always outperforms the Wiener filter. The tests using simulated data define data containing more than 10000 photons as high light level data. Low light level data include data containing 1000 photons or less. Two different M_t values are used to analyze the simulated data, $M_t = 1$ and $M_t = 100$. A $M_t = 1$ value represents the greatest amount of speckle noise possible in real world LADAR data. $M_t = 100$ represents data with a high SNR which corresponds to a small amount of speckle noise in the data. Multiple statistically independent data sets are generated allowing variance calculations to be performed between the iterative and Wiener filter deconvolution methods. Each method deconvolves an average of 50 statistically independent convolved data sets. The variance is calculated by taking the averaged squared difference between the deconvolved data sets and the true target surface location and dividing by the size of the deconvolved data.

Figure 4.12 shows the convolution of the pulse with the front surface of the target for a high light level environment and $M_t = 100$. The location of the target surface appears to be between the 5th and 9th frame based on the location of the peak value of photons. The peak photon quantity will not necessarily correspond to a target surface because the convolution operation most likely causes a data shift from the target's true surface location.

Figure 4.13 displays the non-negative, properly scaled, Wiener filter deconvolved solution for the target's front surface. According to the location of the maximum number of photons from the Wiener filter data, the target's front surface is located in the 6th frame of the data set. The average of the 10000th deconvolved iteration for 50 independent data sets containing the front surface is plotted in Figure 4.14. Based on the average of the final iteration deconvolved data, the target's front surface location is in the 6th frame of the data set.

Both deconvolution methods using simulated data with high light levels and high M_t provide approximately the same estimate for the target's front surface. However, the mean square error difference between the deconvolved profiles from both methods and the true location of the surface show that the iterative algorithm generates a better estimation of the target's front surface. The

mean squared error calculations for both deconvolution methods are illustrated in Figure 4.15. The Wiener filter's maximum variance is approximately 1.8 times larger than the maximum variance of the iterative algorithm. The temporal resolution improvement of the profile due to the Wiener filter is almost negligible.

Comparable results are found when testing high light level, high M_t convolved data containing the target's back surface. Figure 4.16 displays the convolution of the pulse with the back surface of the target. The peak photon value occurs in the 12th frame of the data, but the location of the target surface cannot be determined from observations of the convolved data.

Figure 4.17 contains the Wiener filter deconvolved solution for the target's back surface. According to the Wiener filter data, the target's back surface is located in the 8th frame of the data set. The average of the 10000th deconvolved iteration for 50 independent data sets containing the front surface is shown in Figure 4.18. Based on the average of the final iteration deconvolved data, the target's back surface location is in the 10th frame of the data set.

Both deconvolution methods provide approximately the same estimate for the target's front surface. However, the two methods have a two frame difference for the location of the target's back surface. The mean square error difference between the deconvolved profiles from both methods and the true location of the surface show that the iterative algorithm generates a better estimation of the target's back surface. The variance calculations for both deconvolution methods are illustrated in Figure 4.19. The Wiener filter's maximum variance is approximately 1.5 times larger than the maximum variance of the iterative algorithm. Again, the Wiener filter does a poor job improving the range resolution of the data.

The performance of both methods suffer when testing low light level data with $M_t = 100$. Both methods seem to degrade linearly in low light environments, but the iterative method still deconvolves the data better than the Wiener filter. Figure 4.20 displays the convolution of the pulse with the front surface of the target in a low light level environment. Based on the convolved data profile, the surface appears to be in the 6th or 7th data frame.

The Wiener filter deconvolved data is plotted in Figure 4.21. Based on the Wiener filter results, the target's front surface is located in the 6th frame of the data set. Figure 4.22 shows the average of the 10000th deconvolved iteration for 50 independent data sets containing the front surface. Based on the average of the final iteration deconvolved data, the target's front surface location is in the 6th frame of the data set. The width of the peak of the low light level deconvolved data is much wider than the width of high light level data. Increasing the number of iterations from 10000 to 20000 does not cause the estimated surface location to converge any further.

Both methods provide approximately the same estimate for the target's front surface. As observed with the data above, the variance between the deconvolved profiles from both methods and the true location of the surface show that the iterative algorithm generates a better estimation of the target's front surface. The variance calculations for both deconvolution methods are illustrated in Figure 4.23. The Wiener filter's maximum variance is approximately 1.5 times larger than the maximum variance of the iterative algorithm. Similar to the results given in Figure 4.15 and Figure 4.19, the Wiener filtered profile's temporal resolution is not much better than the original convolved profile.

Similar results to the front surface data are found when testing low light level, high M_t convolved data containing the target's back surface. Figure 4.24 displays the convolution of the pulse with the back surface of the target. The location of the target's back surface is completely masked in the convolved data. The Wiener filter deconvolved back surface data for the low light, $M_t = 100$ case is presented in Figure 4.25. Based on these results, the target's back surface is located in the 8th frame of the data set. The average of the 10000th deconvolved iteration for 50 independent data sets containing the target's back surface is shown in Figure 4.26 Based on the average of the final iteration deconvolved data, the target's back surface is located in the 10th frame of the data set.

Both deconvolution methods provide approximately the same estimate for the target's back surface. However, the two methods have a two frame difference for the location of the target's back surface. This two frame difference is consistent with the analysis performed using the high light

level, $M_t = 100$, data containing the target's back surface. The variance between the deconvolved profiles from both methods and the true location of the surface show that the iterative algorithm generates a better estimation of the target's back surface. The iterative algorithm's lower variance suggests the true back surface of the target is located in the 10th frame of the data set. Based on the variance calculations for both deconvolution methods and the convolved profile in Figure 4.27, the Wiener filter has relatively no effect on the convolved data. The Wiener filter's maximum variance value is approximately 1.76 times larger than the maximum variance of the iterative algorithm for this case.

Now that both high and low light level deconvolved data when $M_t = 100$ has been analyzed, high and low light level data when $M_t = 1$ is considered. Figure 4.28 shows the convolution of the pulse with the front surface of the target for a high light level environment when $M_t = 1$. Figure 4.29 illustrates the Wiener filter deconvolved profile for the target's front surface. According to the Wiener filter data, the target's front surface is approximately located in the 6th frame of the data set.

The average of the 10000th iteration for 50 independent data sets containing the front surface is provided in Figure 4.30. Based on the average of the final iteration deconvolved data, the target's front surface appears to be located in the 6th frame of the data set. The low speckle noise parameter value increases the width of the deconvolved profile compared to the iterative deconvolved data shown in Figure 4.14 when $M_t = 100$.

The high light deconvolved data when $M_t = 1$ is similar to high light deconvolved data when $M_t = 100$. Both deconvolution methods provide approximately the same estimate for the target's front surface. The variance of the deconvolved profiles from both methods and the true location of the surface show that the iterative algorithm generates a better estimation of the target's front surface. In fact the variance calculations for both deconvolution methods are illustrated in Figure 4.31 show that the Wiener filter actually decreases the temporal resolution of convolved profile. For this case, applying a Wiener filter is detrimental to improving the range resolution of the data.

The Wiener filter's maximum variance value is approximately 2.78 times larger than the maximum variance of the iterative algorithm.

Figure 4.32 displays the convolution of the pulse with the back surface of the target for a high light level environment when $M_t = 1$. The Wiener filter deconvolved profile for the target's back surface is provided in Figure 4.33. The target's back surface is approximately located in the 8th frame of the data set based on the deconvolved profile.

The average of the 10000th iteration for 50 independent data sets containing the front surface is provided in Figure 4.34. Based on the average of the final iteration deconvolved data, the target's back surface appears to be approximately located in the 9th frame of the data set. Again, the iterative deconvolved profiles resulting from low M_t values have an increased width compared to corresponding iterative deconvolved data with high M_t values as shown in Figure 4.18.

The variance between the deconvolved profiles from both methods and the true location of the surface again show that the iterative algorithm generates a superior estimation of the target's back surface. The variance calculations for both deconvolution methods are illustrated in Figure 4.35. The results in Figure 4.35 mirror the results shown in Figure 4.31. The Wiener filter lessens the range resolution of the convolved pulse profile. The Wiener filter's maximum variance value is approximately 1.78 times larger than the maximum variance of the iterative algorithm.

Figure 4.36 shows the convolved data containing the target's front surface for a low light level environment when $M_t = 1$. This data set represents one of the the most challenging noise environments possible to test the deconvolution methods. The Wiener filter deconvolved data is displayed in Figure 4.37. Based on the Wiener filter results, the target's front surface is approximately located in the 6th frame of the data set. The average of the 10000th deconvolved iteration for 50 independent data sets containing the front surface is illustrated in Figure 4.38. Based on the average of the final iteration deconvolved data, the target's front surface is located in the 6th frame of the data set. The width of the peak of the low light level deconvolved data when $M_t = 1$ is much wider compared to the deconvolved profiles of high light level data when $M_t = 100$.

The variance between the deconvolved profiles from both methods and the true location of the surface for this data show that the iterative algorithm generates a better estimate of the target's front surface. The variance calculations for both deconvolution methods are provided in Figure 4.39. The Wiener filter's maximum variance is approximately 1.36 times larger than the maximum variance of the iterative algorithm.

The last data set analyzed is low light level data containing the target's back surface when $M_t = 1$. Figure 4.40 plots the convolution of the pulse with the back surface. Figure 4.41 shows the Wiener filter deconvolved profile for the target's back surface. The target's back surface is approximately located in the 8th frame of the data set based on the deconvolved profile. The average of the 10000th iteration for 50 independent data sets containing the front surface is plotted in Figure 4.42. Based on the average of the final iteration deconvolved data, the target's back surface is located in the 10th frame of the data set.

The variance between the deconvolved profiles from both methods and the true location of the surface again show that the iterative algorithm generates better estimation of the target's back surface. The variance values for both deconvolution methods and the convolved pulse profile are illustrated in Figure 4.43. The results for this case show that the Wiener filter negatively impacts the range resolution of the data. The Wiener filter's maximum variance is approximately 2.0 times larger than the maximum variance of the iterative algorithm. A summary of the measured and simulated data deconvolution results are provided in Table 4.1 and Table 4.2.

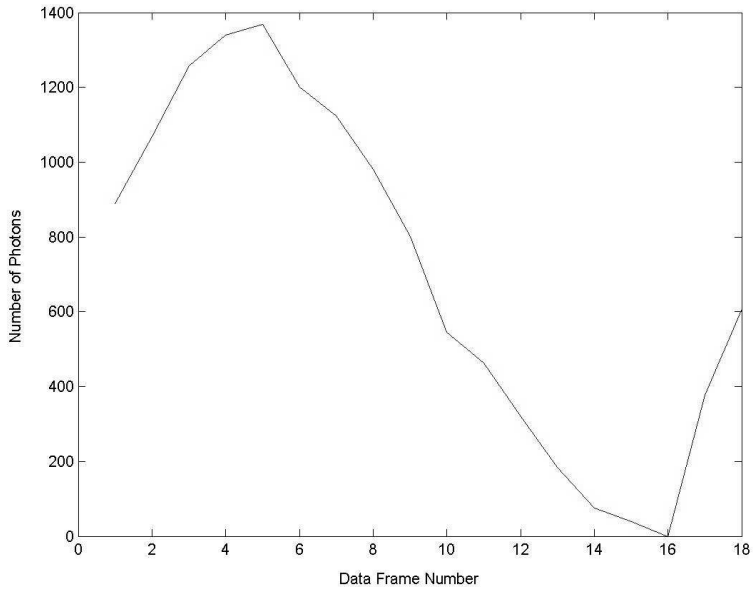

Figure 4.1: Convolved measured data containing the front surface of the target after pre-processing has been performed. The signal to noise ratio of data appears to be relatively high so the target surface could be estimated from the convolved profile. However, effects due to the convolution operation on the data adds some uncertainty as to the exact frame of the target surface location.

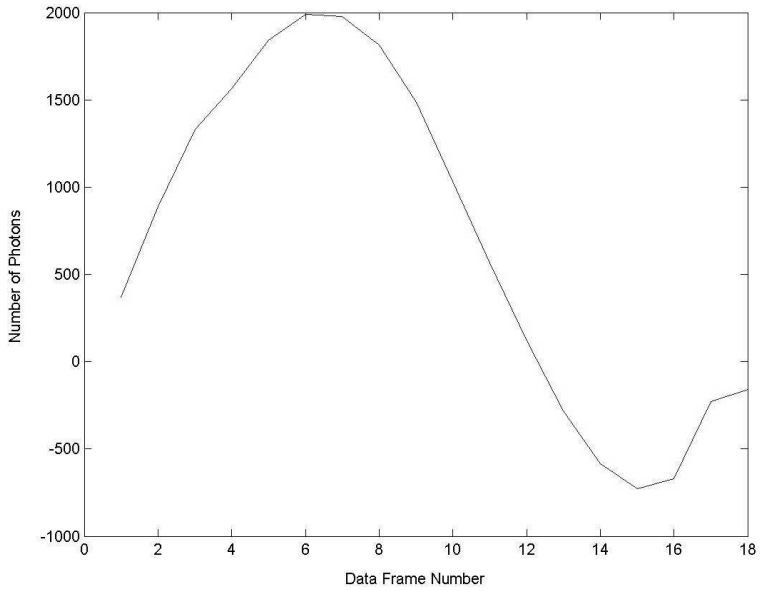

Figure 4.2: The Wiener filter deconvolved target data. This deconvolved profile contains negative values due to the nature of the Wiener filter and the shape of the convolved data. In order to properly show the true Wiener filtered solution, the negative values are set to zero, and the entire deconvolved profile is scaled appropriately to show a conservation of photons between the convolved and deconvolved target surfaces.

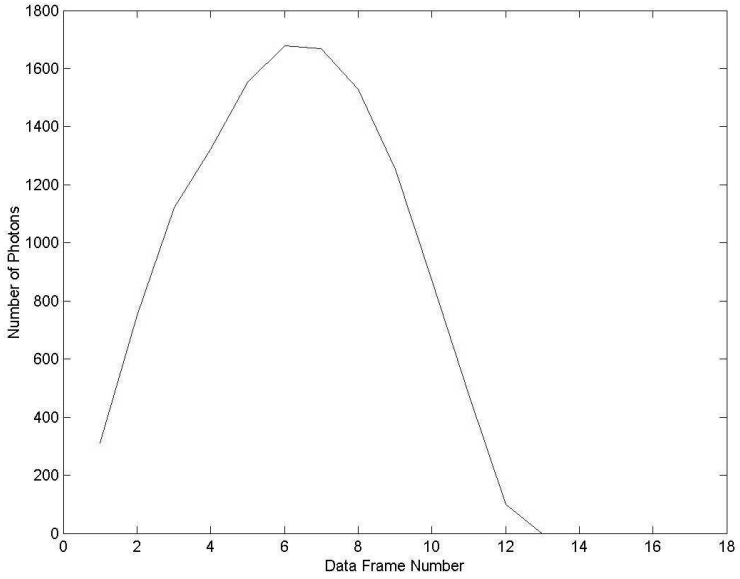

Figure 4.3: The true Wiener filter deconvolved target data after removing negative values and properly scaling the data. The data was scaled based on conserving the total number of photons between the convolved and deconvolved data sets.

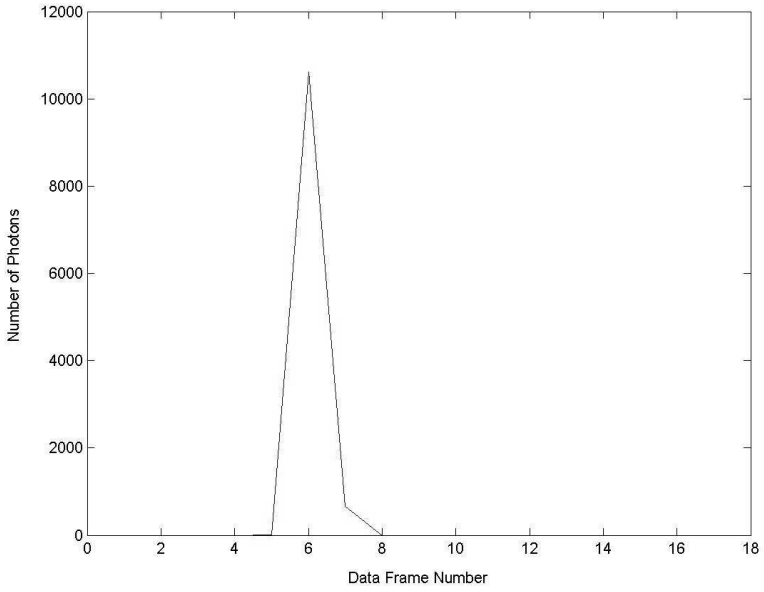

Figure 4.4: Final iterative solution (10000th iteration) for the data containing the front surface of the target. The surface is located in the 6th frame of the data set.

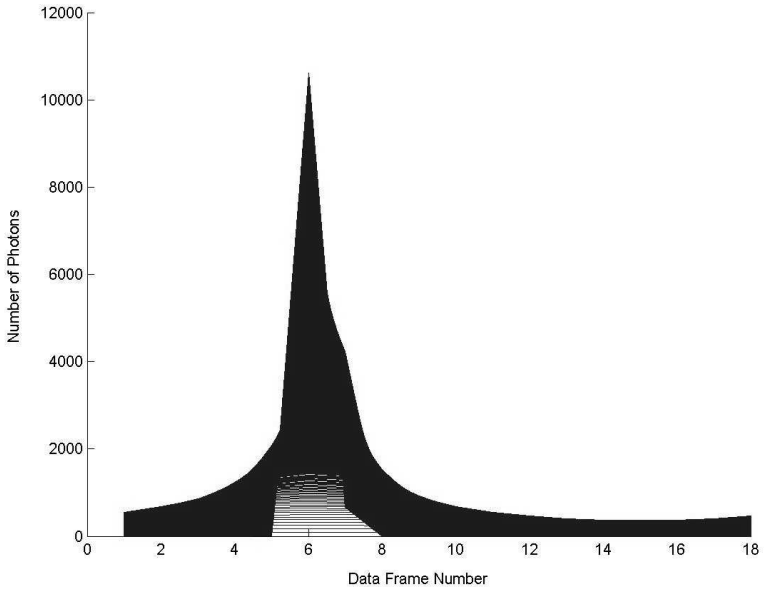

Figure 4.5: All 10000 iterations of the iterative algorithm deconvolved data. The iterations show the solution converging on the frame location containing the target's front surface.

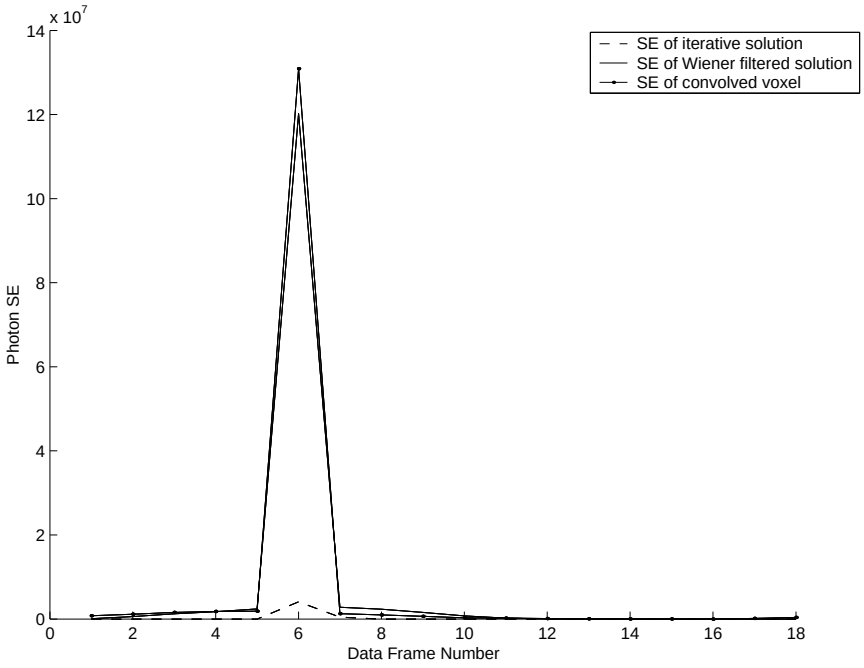

Figure 4.6: Squared error calculations between both deconvolved profiles, the convolved profile, and the target's front surface in the true scene. The iterative algorithm outperforms the Wiener filter significantly. The Wiener filter's maximum SE value is approximately 29.3 times larger than the maximum SE of the iterative algorithm.

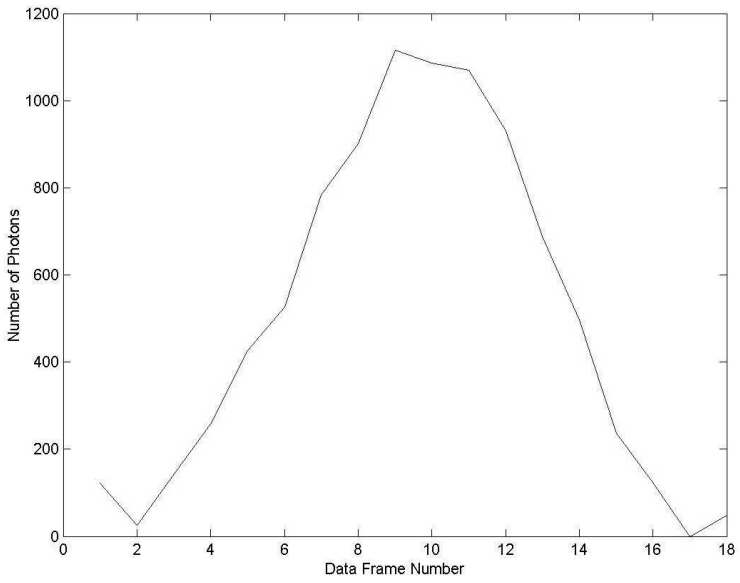

Figure 4.7: Convolved measured data containing the back surface of the target after pre-processing has been performed. Again, the signal to noise ratio of the data appears to be relatively high, so the target surface could be estimated from the convolved profile. However, effects resulting from the convolution operation on the data adds some uncertainty as to the exact frame of the target surface location.

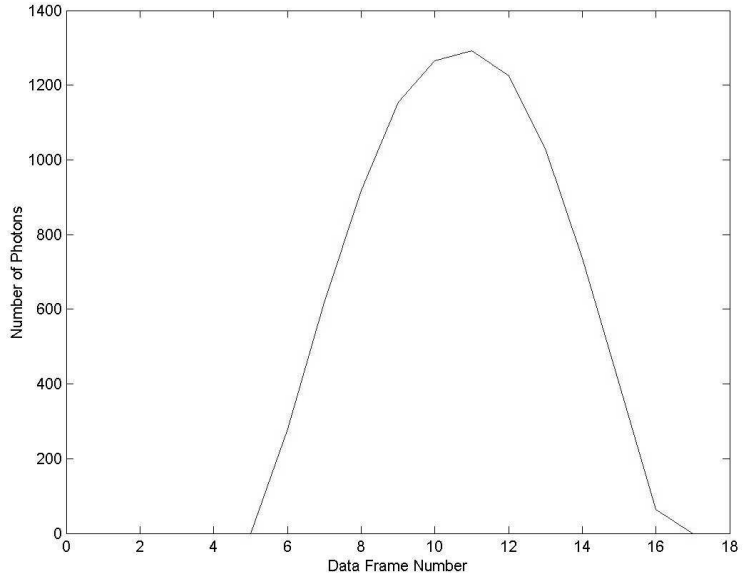

Figure 4.8: The true Wiener filter deconvolved target data after removing negative values and properly scaling the data. The data was scaled based on conserving the total number of photons between the convolved and deconvolved data sets. The target's back surface approximate location is in the 11th frame of the data set.

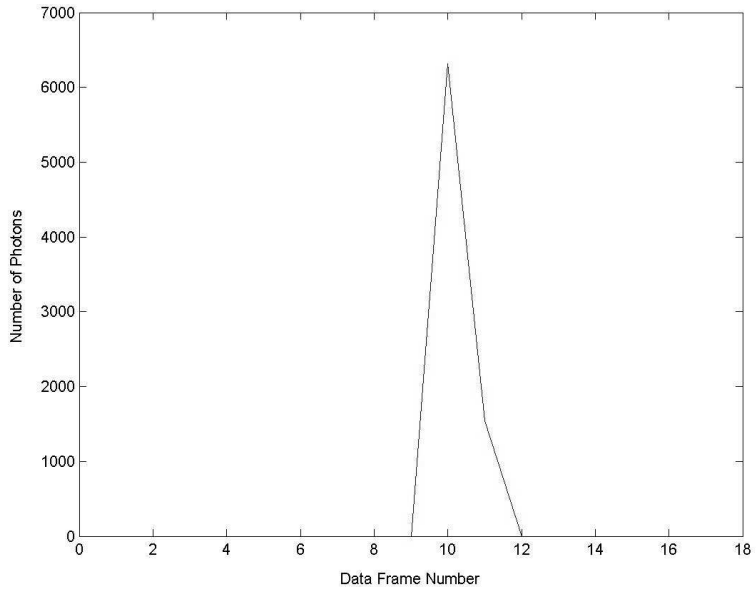

Figure 4.9: Final iterative solution(10000th iteration) for the data containing the back surface of the target. The surface is located in the 10th frame of the data set.

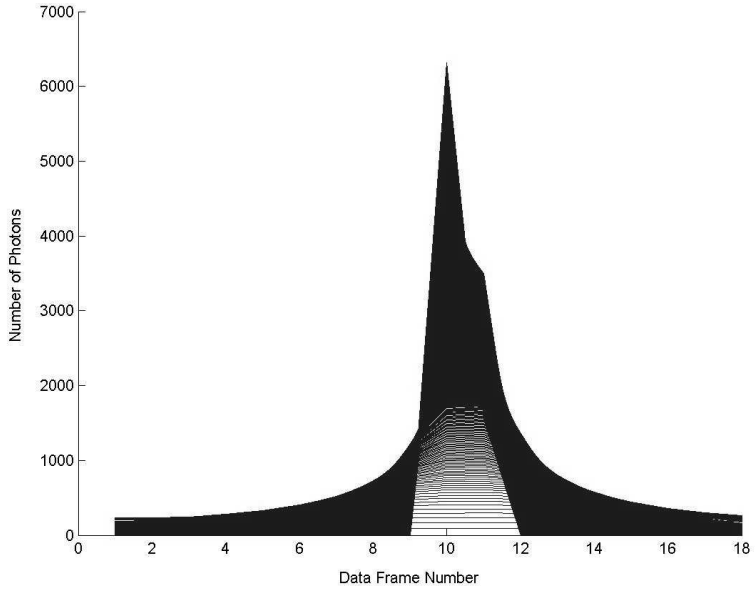

Figure 4.10: All 10000 solutions of the iterative algorithm data. The iterations show the solution converging on the frame location containing the target's back surface.

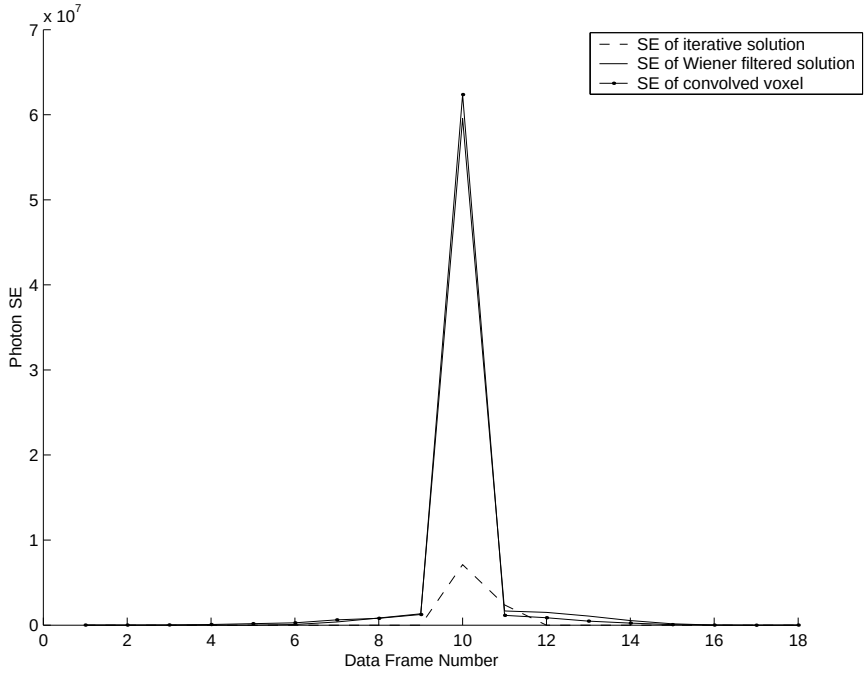

Figure 4.11: Squared error calculations between both deconvolved profiles, the convolved profiles, and the target's back surface in the true scene. The iterative algorithm substantially outperforms the Wiener filter. The Wiener filter's maximum SE value is approximately 8.4 times larger than the maximum SE of the iterative algorithm.

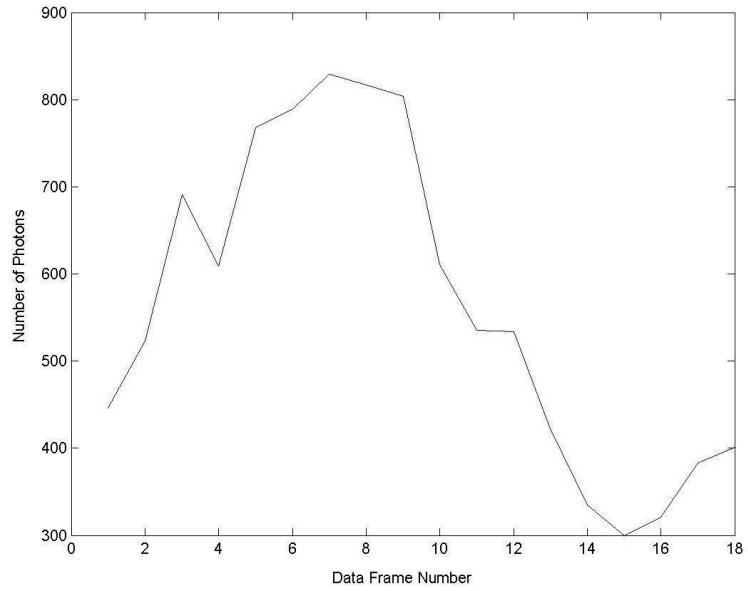

Figure 4.12: $M_t = 100$. High light level convolved data containing the front surface of the target after pre-processing has been performed. Based on the peak of the data the so the target surface appears to be located somewhere between the 5th and 9th frame in the data set. The convolution operation on the data adds uncertainty as to the exact frame of the target surface location.

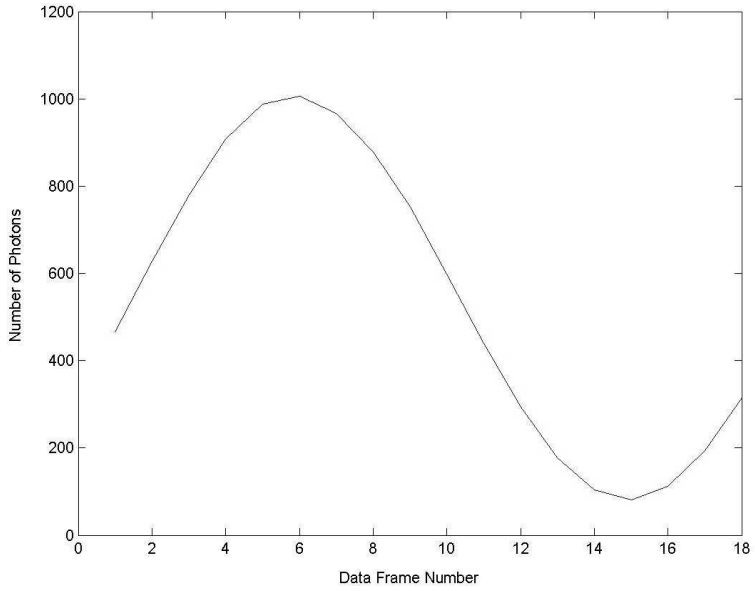

Figure 4.13: $M_t = 100$. High light level Wiener filter deconvolved target data after removing negative values and properly scaling the data. The data was scaled based on conservation of the total number of photons between the convolved and deconvolved data sets.

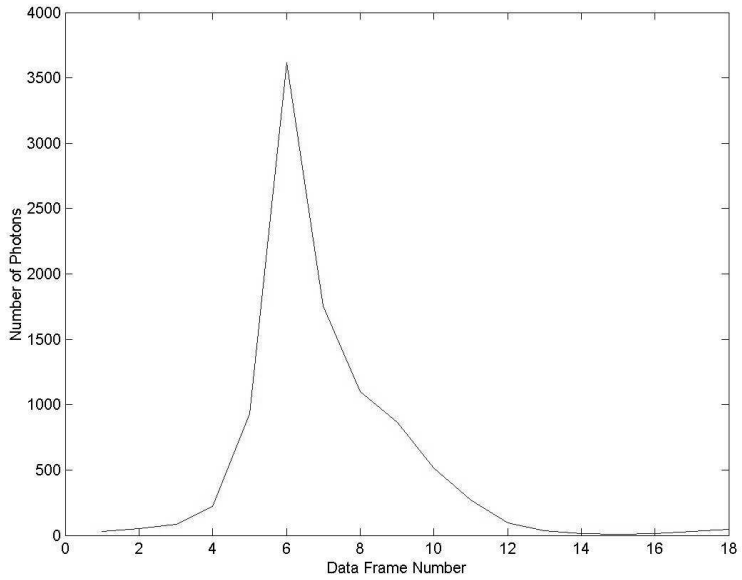

Figure 4.14: $M_t = 100$, high light level data. Average of the final deconvolved iteration (10000th iteration) for 50 independent data sets. The surface is located in the 6th frame of the data set.

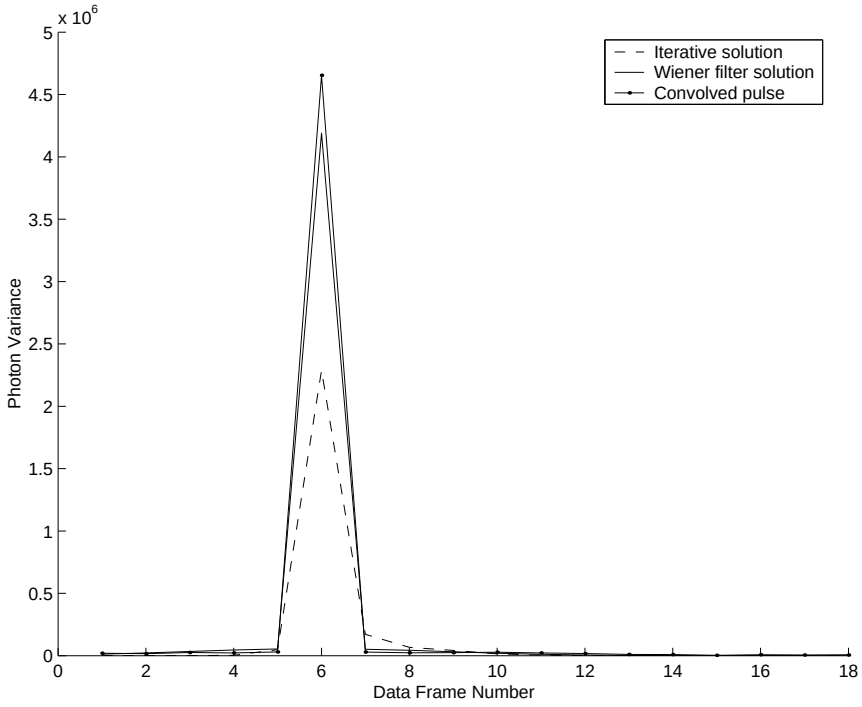

Figure 4.15: $M_t = 100$, high light level data. Variance calculations for both deconvolution methods and the convolved profile. The iterative algorithm outperforms the Wiener filter considerably. The Wiener filter's maximum variance is approximately 1.8 times larger than the maximum variance of the iterative algorithm for this case.

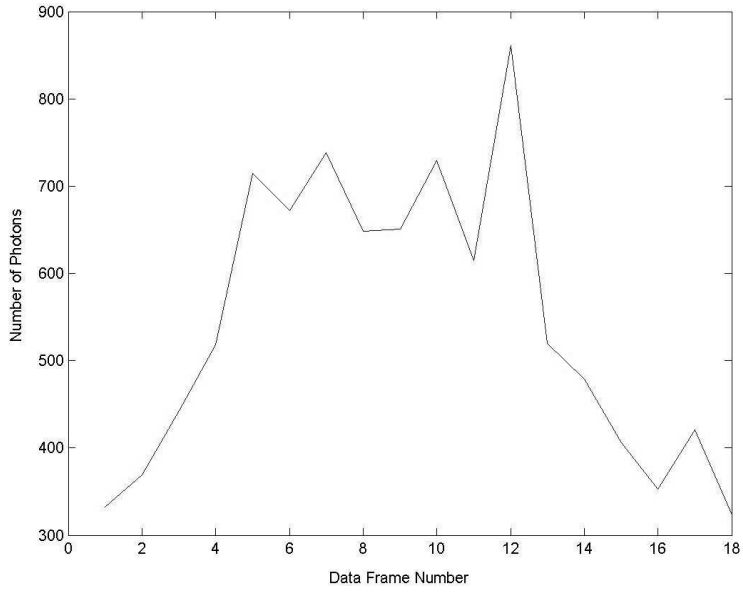

Figure 4.16: $M_t = 100$. High light level convolved data containing the back surface of the target. Finding the target surface is difficult from observing only the convolved data.

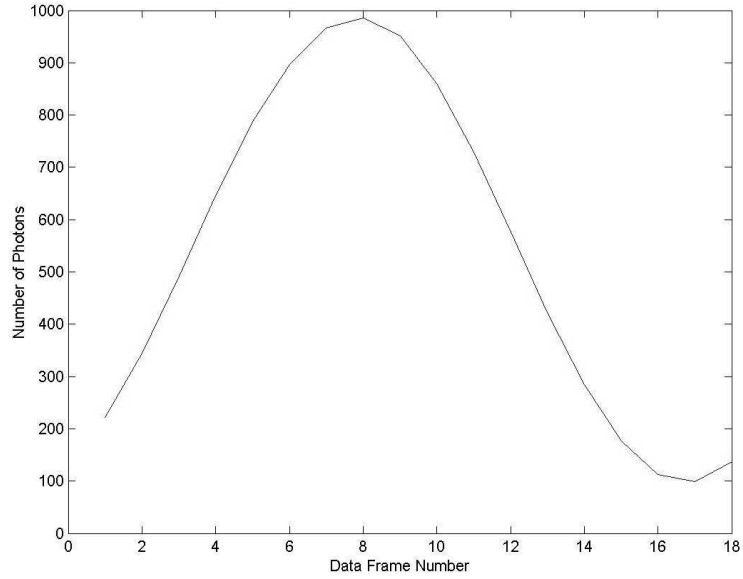

Figure 4.17: High light level Wiener filter deconvolved target data. The target's back surface based on the Wiener filter solution is in the 8th frame of the data.

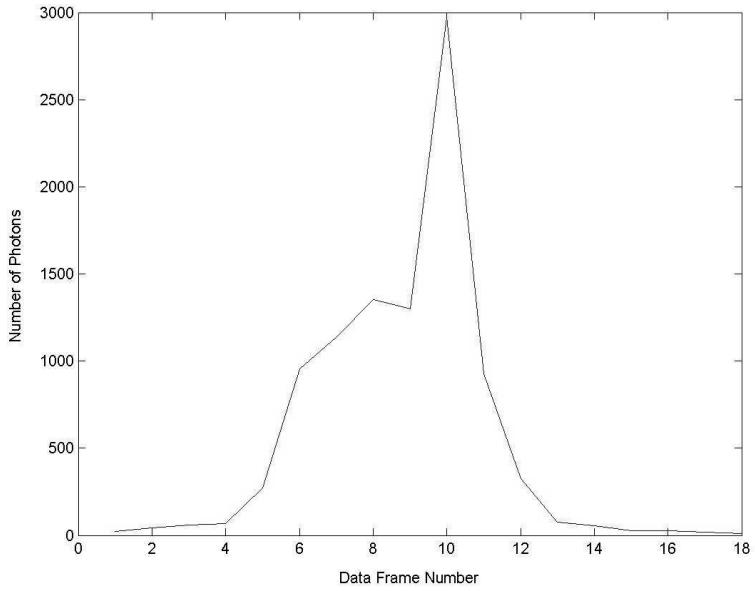

Figure 4.18: $M_t = 100$, high light level data. Average of the final deconvolved iteration (10000th iteration) for 50 independent data sets. The surface is located in the 10th frame of the data set.

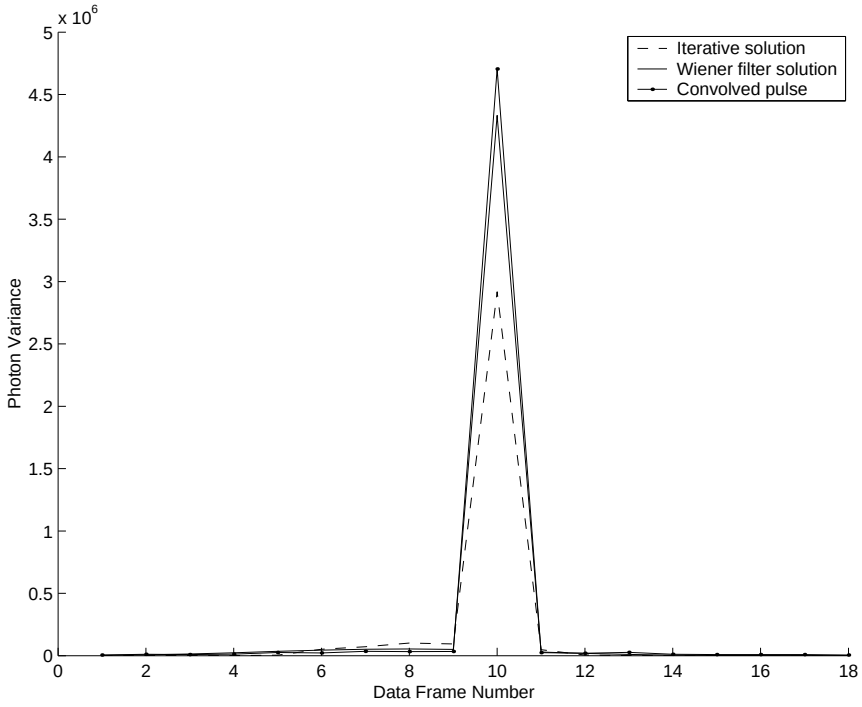

Figure 4.19: $M_t = 100$, high light level data. Variance for both deconvolution methods and the convolved pulse profile. The Wiener filtered profile's MSE is nearly identical to the convolved profile's MSE. The Wiener filter's maximum variance is approximately 1.5 times larger than the iterative algorithm's maximum variance.

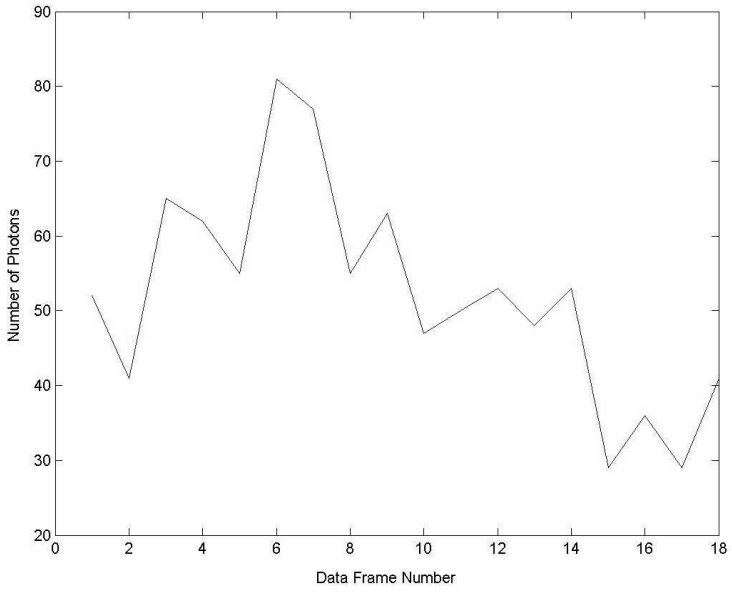

Figure 4.20: $M_t = 100$. Low light level convolved data containing the front surface of the target. The target surface appears to be located in the 6th or 7th data frame.

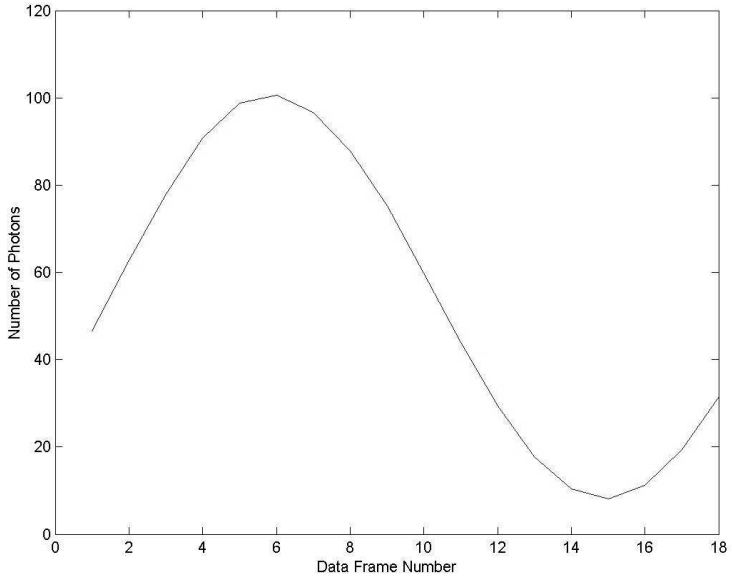

Figure 4.21: $M_t = 100$. Low light level, Wiener filter deconvolved target data after removing negative values and proper scaling. The front surface of the target is approximately located in the 6th frame of the data set.

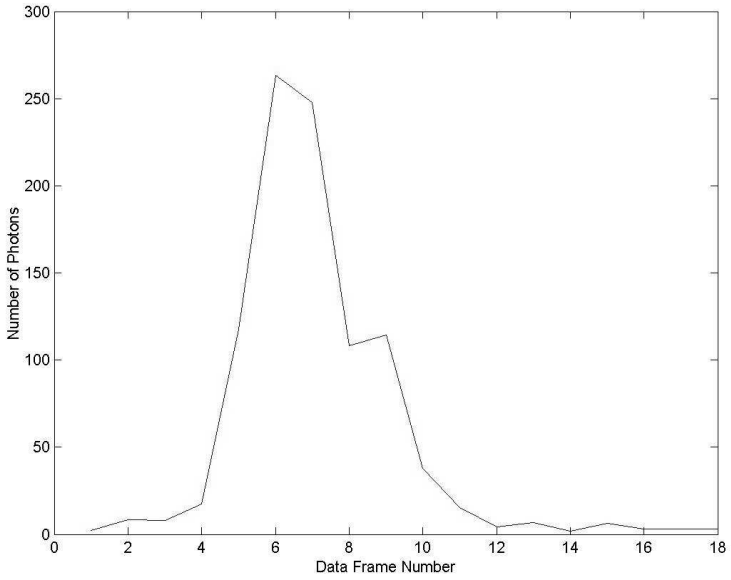

Figure 4.22: $M_t = 100$, low light level data. Average of the final deconvolved iteration (10000th iteration) for 50 independent data sets. The surface is located in the 6th frame of the data set.

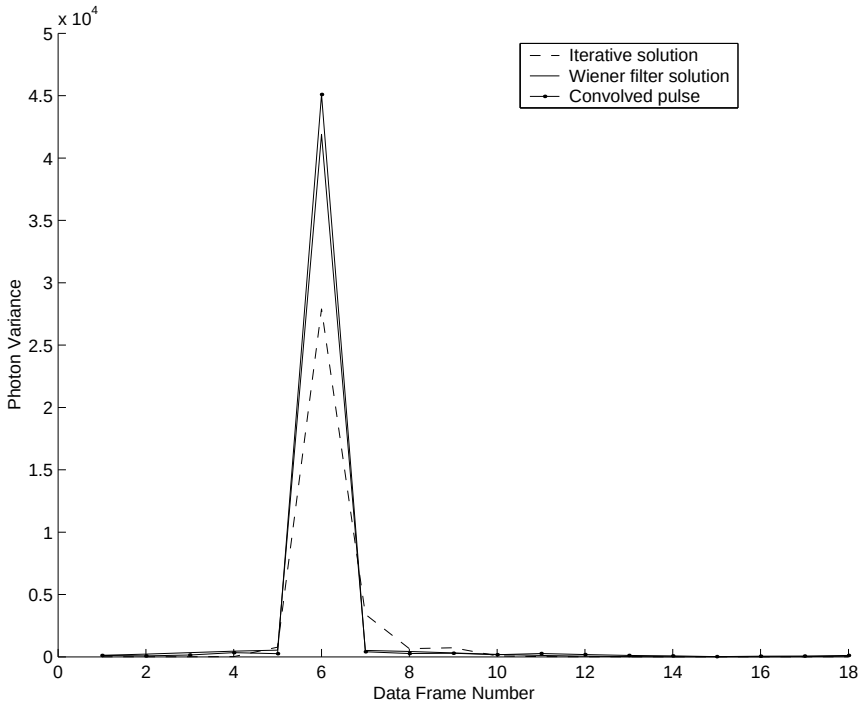

Figure 4.23: $M_t = 100$, high light level data. Variance for both deconvolution methods and the convolved profile. The iterative algorithm does a very good job improving the temporal resolution of the data compared to the Wiener filter. The Wiener filter's maximum variance is approximately 1.5 times larger than the maximum variance of the iterative algorithm for this case.

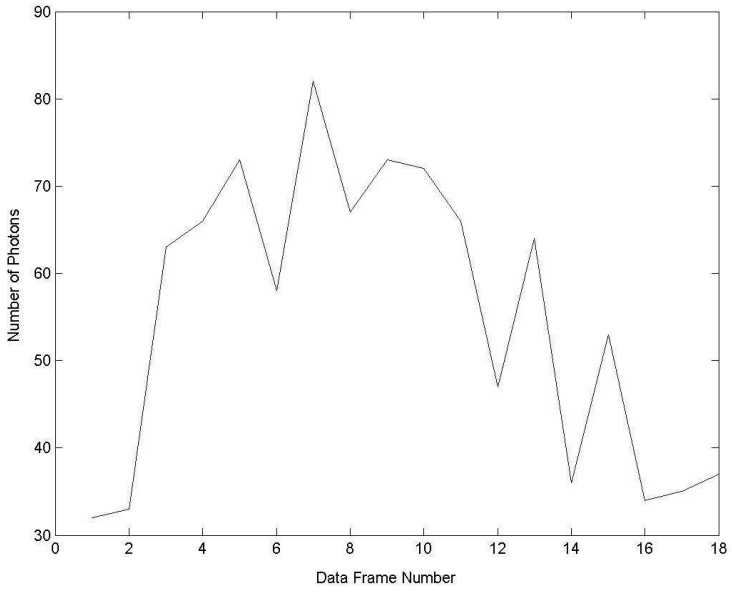

Figure 4.24: $M_t = 100$. Low light level convolved data containing the back surface of the target. The surface location is completely imperceptible in the convolved data.

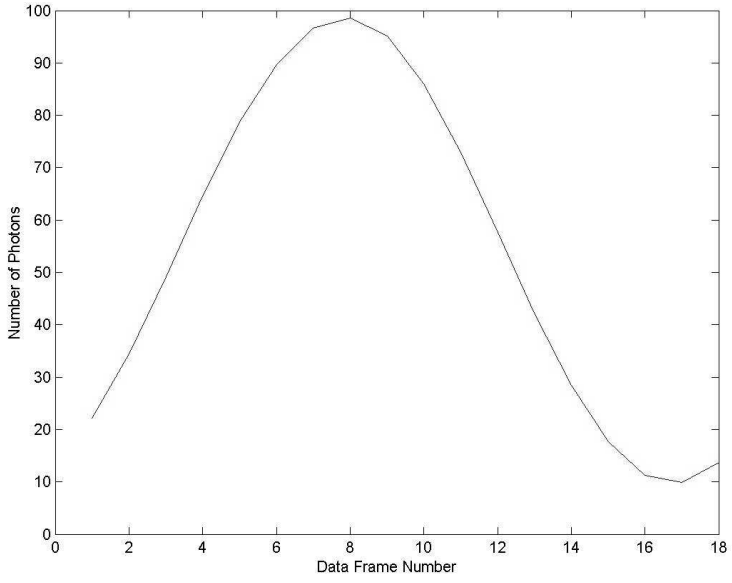

Figure 4.25: $M_t = 100$. Low light level, Wiener filter deconvolved target data after removing negative values and proper scaling. The back surface of the target is approximately located in the 8th frame of the data set.

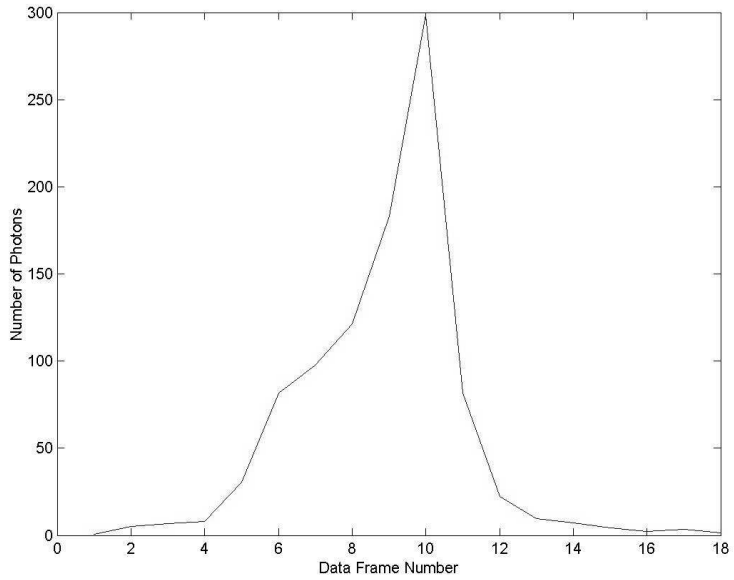

Figure 4.26: $M_t = 100$, low light level data. Average of the final deconvolved iteration (10000th iteration) for 50 independent data sets. The surface is located in the 10th frame of the data set.

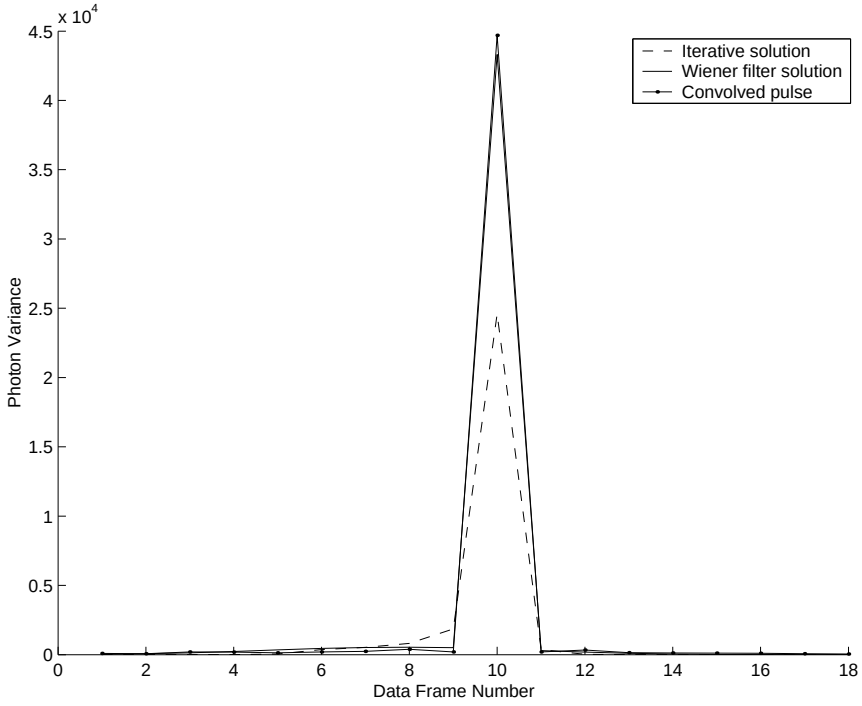

Figure 4.27: $M_t = 100$, low light level data. Variance for the convolved pulse profile and both deconvolution methods. The iterative algorithm temporally resolves the data better than the Wiener filter. The Wiener filtered profile's maximum variance is approximately 1.76 times larger than the maximum variance of the iterative algorithm profile for this case.

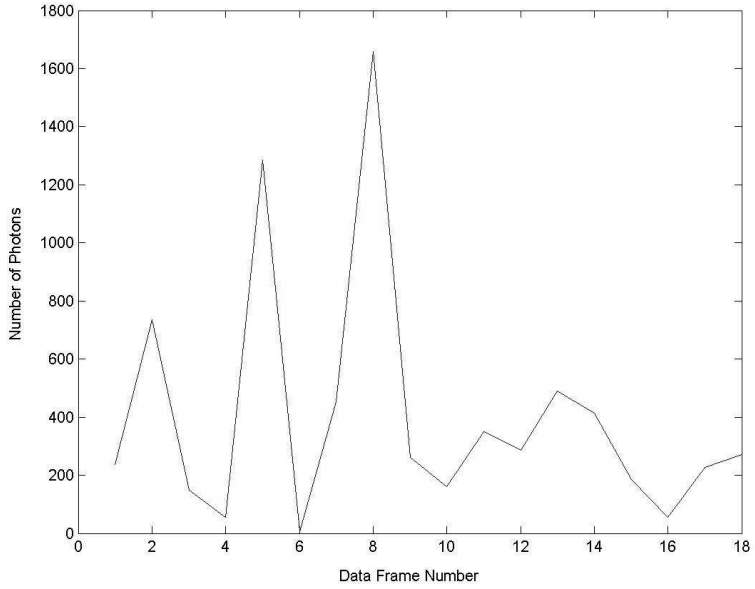

Figure 4.28: $M_t = 1$. High light level convolved data containing the front surface of the target after pre-processing has been performed. Even in a high light level environment, locating the target's surface in the convolved data is difficult if the M_t value is small.

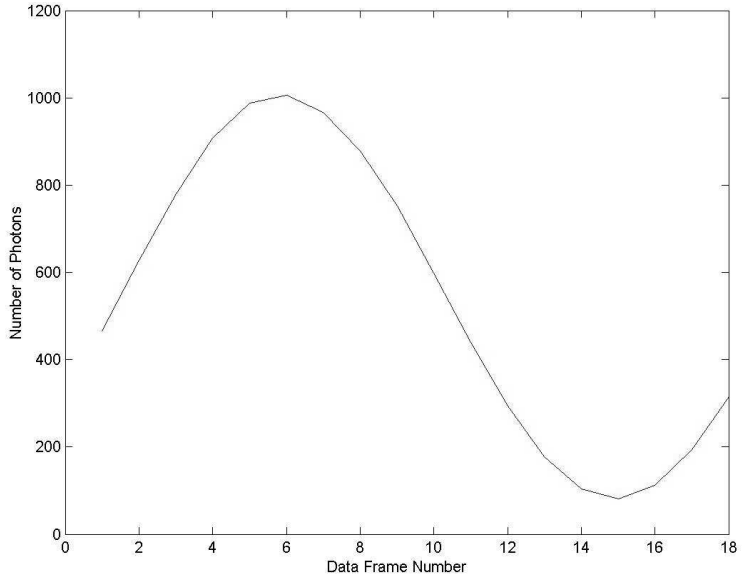

Figure 4.29: $M_t = 1$. High light level Wiener filter deconvolved target data. Based on the results, the target's front surface is located in the 6th frame of the data set.

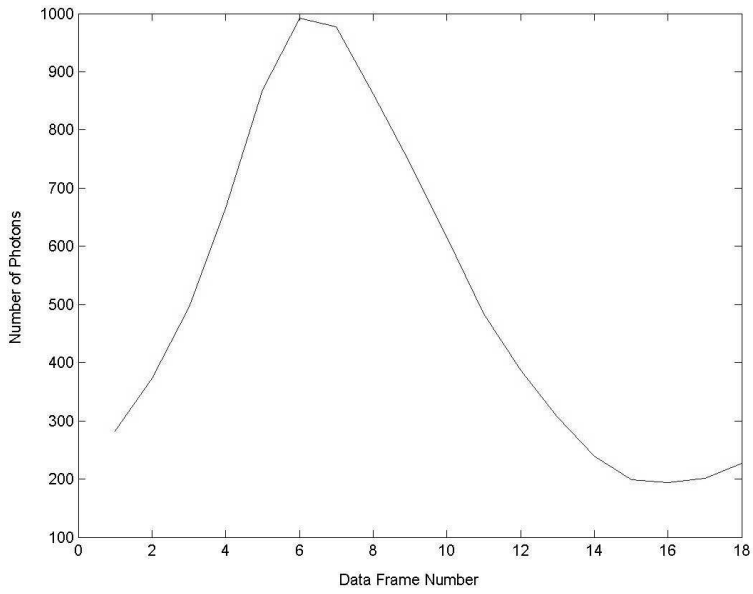

Figure 4.30: $M_t = 1$, high light level data. Average of the final deconvolved iteration (10000th iteration) for 50 independent data sets. The target's front surface is located in the 6th frame of the data set. The low speckle noise parameter value increases the width of the deconvolved profile compared to the iterative deconvolved data shown in Figure 4.14 when $M_t = 100$.

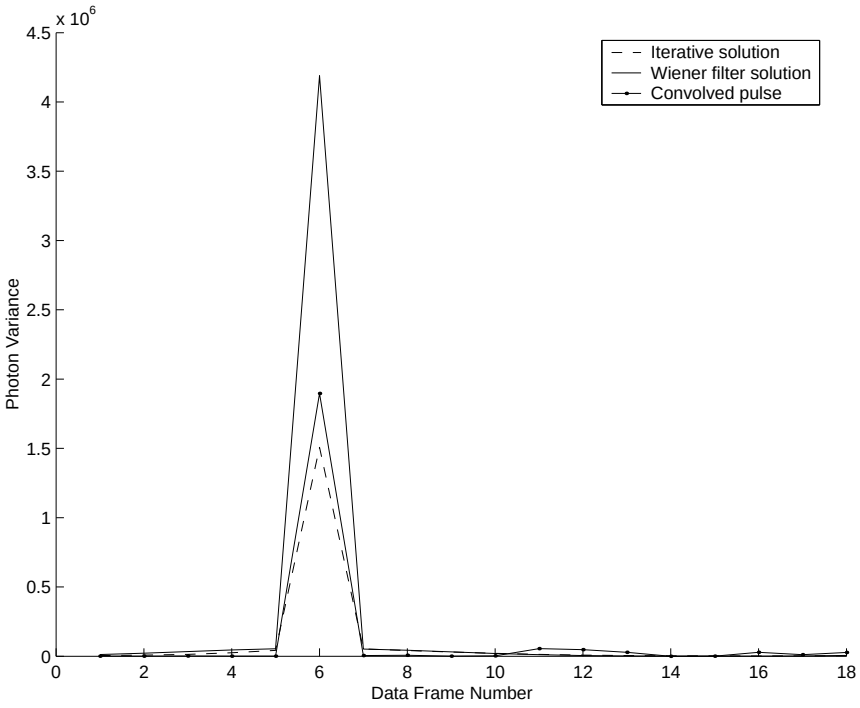

Figure 4.31: $M_t = 1$, high light level data. Variance for both deconvolution methods. Applying the Wiener filter to the pulse profile actually decreases the profile's temporal resolution. The Wiener filter's maximum variance is approximately 2.78 times larger than the maximum variance of the iterative algorithm for this case.

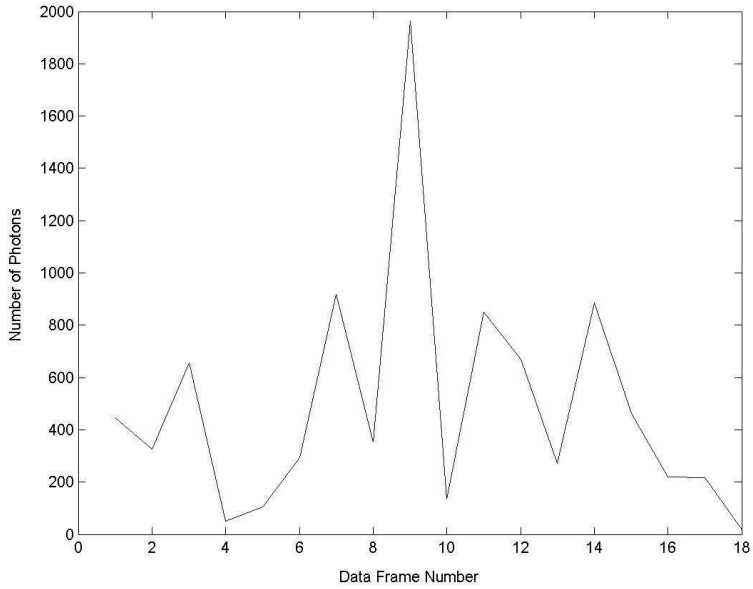

Figure 4.32: $M_t = 1$. High light level convolved data containing the back surface of the target after pre-processing has been performed. Based on the highest peak in the convolved data, the surface appears to be located in the 9th frame of the data set.

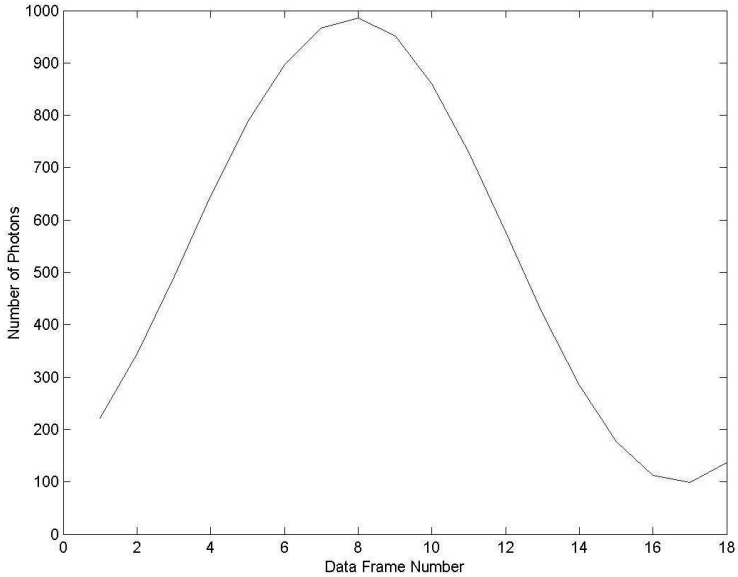

Figure 4.33: $M_t = 1$. High light level Wiener filter deconvolved target data. Based on the results, the target's back surface is located in the 8th frame of the data set.

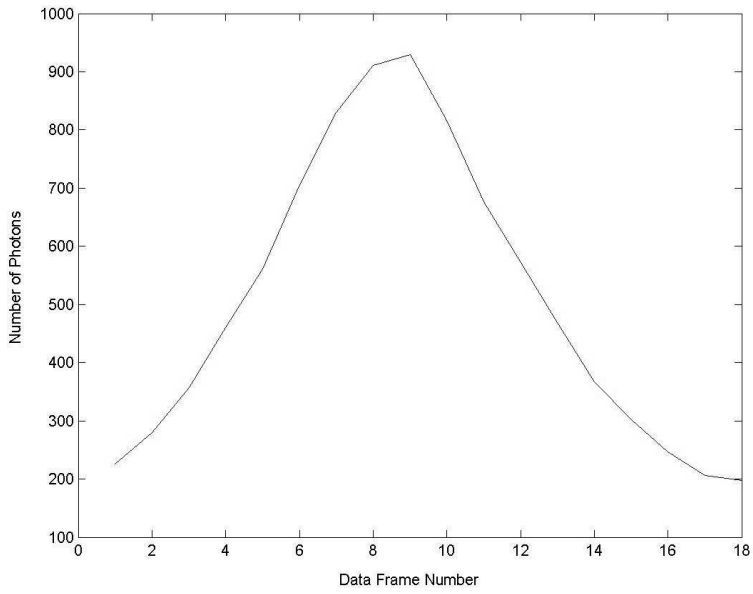

Figure 4.34: $M_t = 1$, high light level data. Average of the final deconvolved iteration (10000th iteration) for 50 independent data sets. The target's back surface is located in the 9th frame of the data set. The low speckle noise parameter value increases the width of the deconvolved profile compared to the iterative deconvolved data shown in Figure 4.18 when $M_t = 100$.

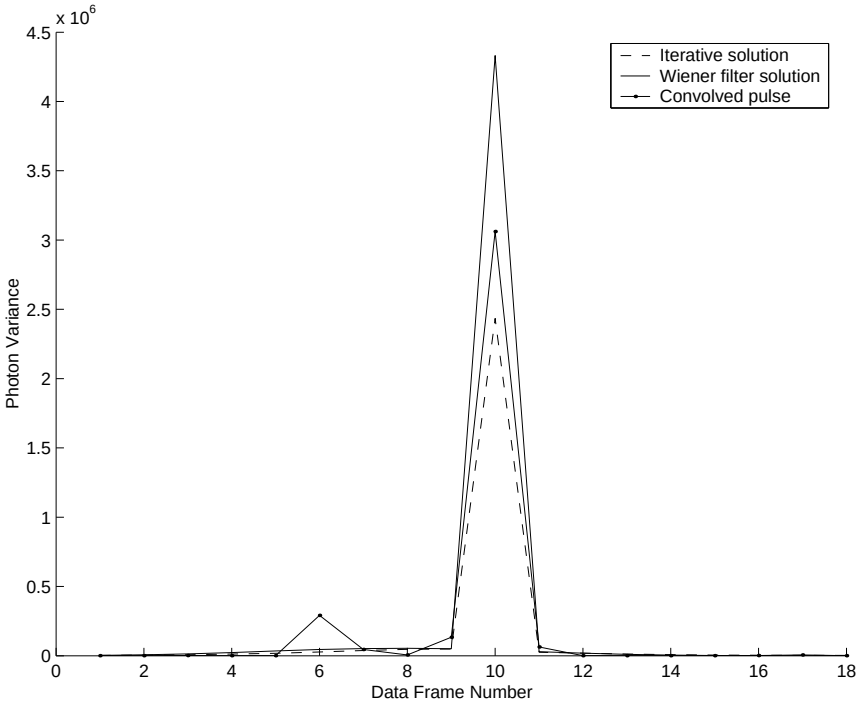

Figure 4.35: $M_t = 1$, high light level data. Variance for both deconvolution methods and the convolved profile. The Wiener causes further range resolution degradation of the pulse profile. The Wiener filter's maximum variance is approximately 1.78 times larger than the maximum variance of the iterative algorithm for this case.

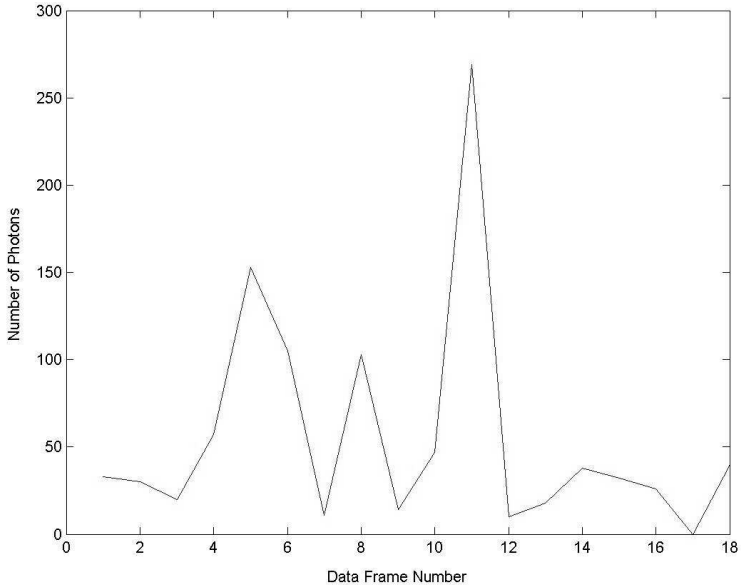

Figure 4.36: $M_t = 1$. Low light level convolved data containing the front surface of the target. The target surface location is indistinguishable in the convolved data.

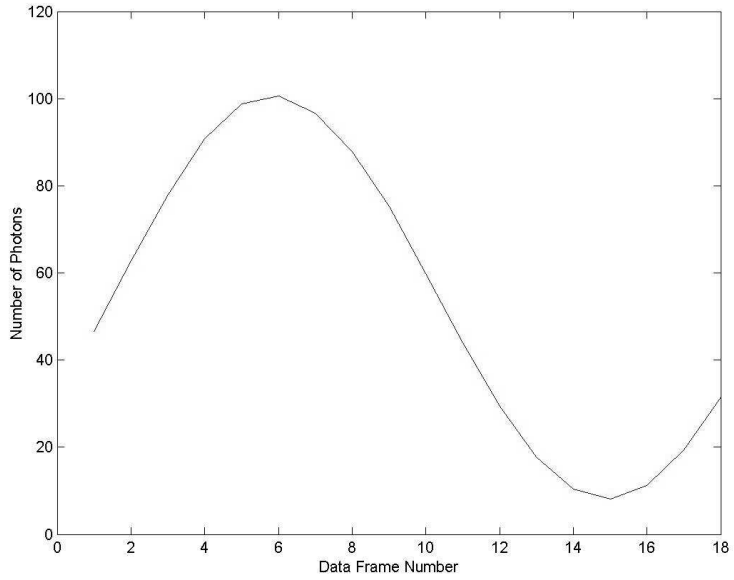

Figure 4.37: $M_t = 1$. Low light level, Wiener filter deconvolved target data after removing negative values and applying the proper scaling. The front surface of the target is approximately located in the 6th frame of the data set.

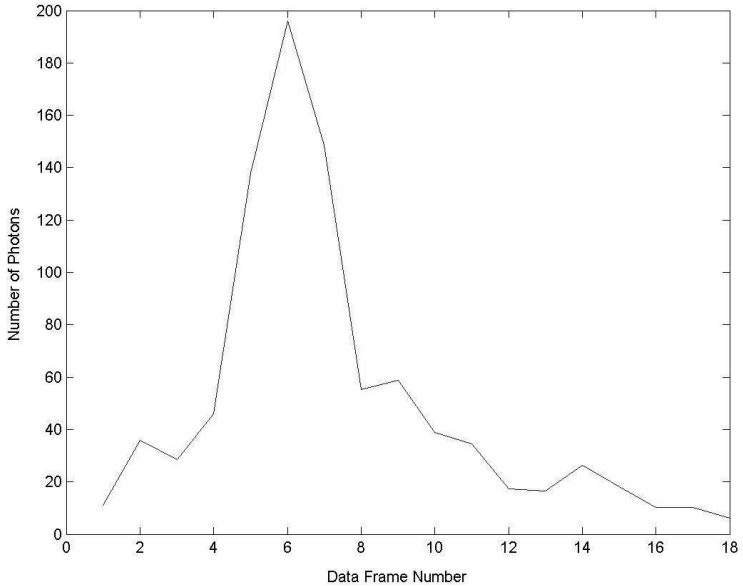

Figure 4.38: $M_t = 1$, low light level data. The averaged final deconvolved iteration (10000th iteration) for 50 independent data sets. The surface is located in the 6th frame of the data set.

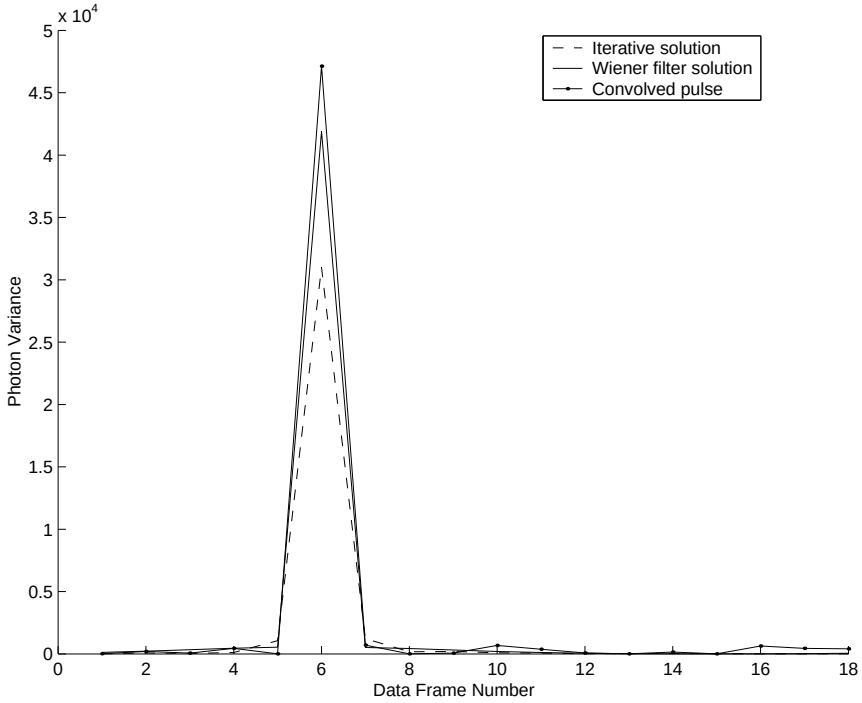

Figure 4.39: $M_t = 1$, low light level data. Variance for both deconvolution methods and the convolved pulse. The Wiener filtered profile shows a slight improvement in temporal resolution compared to the convolved data. The iterative method yields a more favorable estimation of the target's surface location. The Wiener filter's maximum variance is approximately 1.36 times larger than the maximum variance of the iterative algorithm for this case.

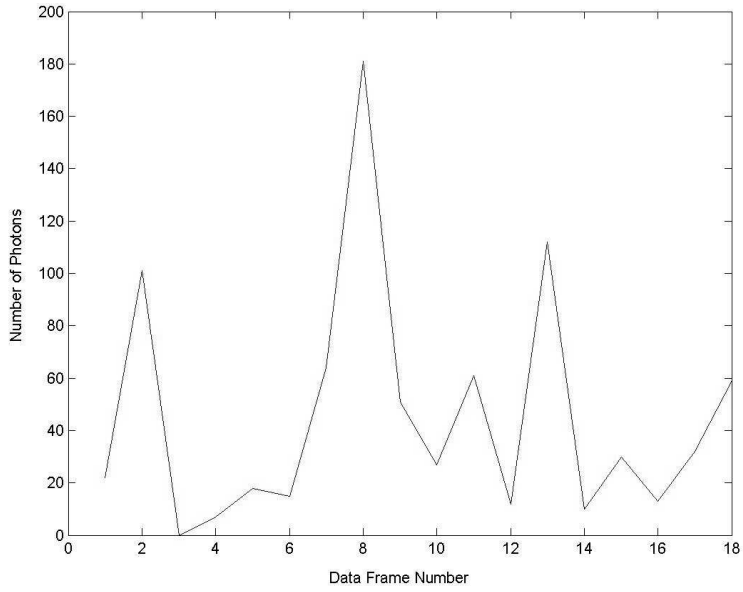

Figure 4.40: $M_t = 1$. Low light level convolved data containing the back surface of the target. Based on the highest peak in the convolved data, the surface appears to be located in the 8th frame of the data set.

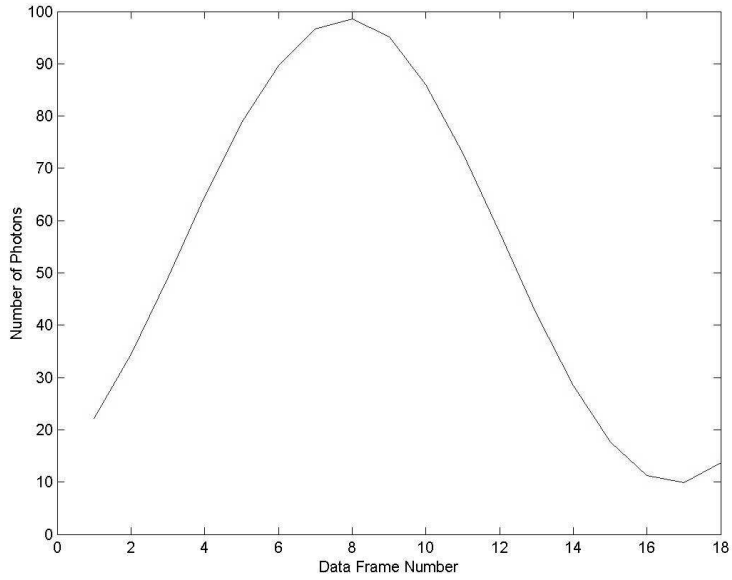

Figure 4.41: $M_t = 1$ low light level Wiener filter deconvolved target data. Based on the results, the target's back surface is located in the 8th frame of the data set.

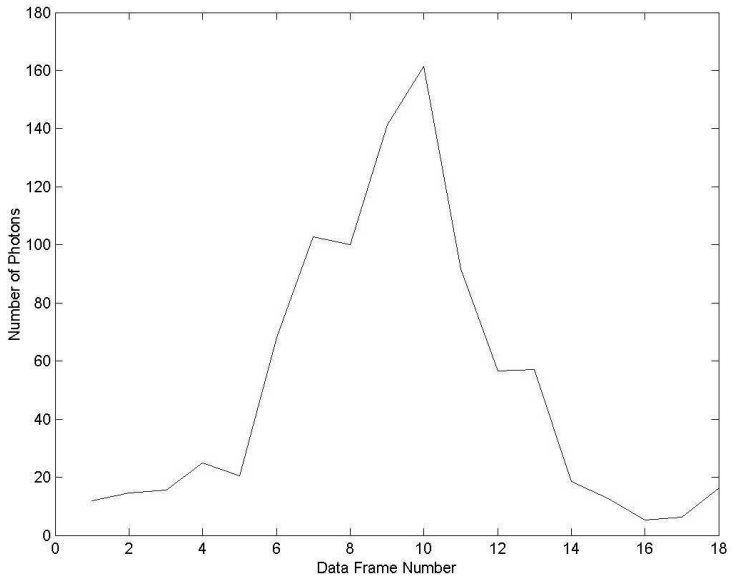

Figure 4.42: $M_t = 1$, low light level data. Average of the final deconvolved iteration (10000th iteration) for 50 independent data sets. The target's back surface is located in the 10th frame of the data set.

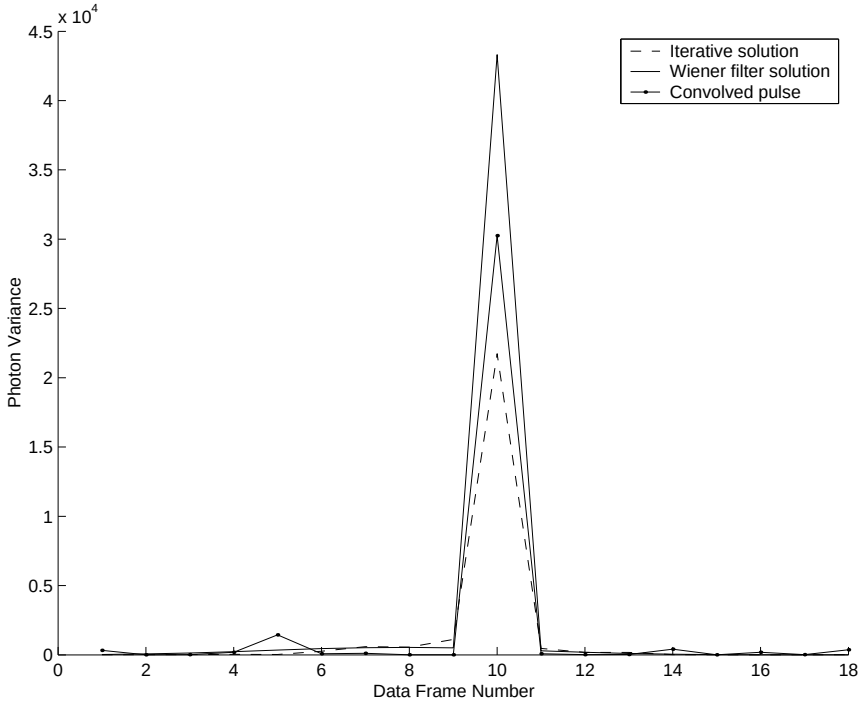

Figure 4.43: $M_t = 1$, low light level data. Variance for both deconvolution methods and the convolved pulse profile. The Wiener worsens the range resolution of the convolved pulse. The Wiener filter's maximum variance is approximately 2.0 times larger than the iterative algorithm's maximum variance for this case.

Table 4.1: Target Surface Locations for Deconvolved Data (W-Wiener filter, I-Iterative algorithm).

Type of data	Front surface (W)	Back Surface (W)	Front Surface (I)	Back Surface (I)
Measured data	6th frame	11th frame	6th frame	10th frame
Simulated data				
High light, $M_t = 100$	6th frame	8th frame	6th frame	10th frame
High light, $M_t = 1$	6th frame	8th frame	6th frame	9th frame
Low light, $M_t = 100$	6th frame	8th frame	6th frame	10th frame
Low light, $M_t = 1$	6th frame	8th frame	6th frame	10th frame

Table 4.2: Weiner Filter to Iterative Algorithm Peak SE and Variance Ratios

Type of Data	Peak SE/Variance Ratios(Front Surface)	Peak SE/Variance Ratios(Back Surface)
Measured data (SE)	29.40	8.40
Simulated data (Variance)		
High light, $M_t = 100$	1.80	1.50
High light, $M_t = 1$	2.78	1.78
Low light, $M_t = 100$	1.50	1.76
Low light, $M_t = 1$	1.36	2.00

V. Conclusions and Additional Research

5.1 Conclusions

Comparing the results of the two deconvolution methods summarized in Table 4.1 and Table 4.2 validate the performance of the iterative algorithm over the Wiener filter. For the simulated data, the iterative algorithm reconstructs the target's front and back surfaces in approximately the same frame locations as those in the original scene. The Wiener filter's reconstruction shortens the distance between the target surfaces compared to the true image. The iterative algorithm also yields a better deconvolved profile for the measured data. The algorithm reconstructs the target surfaces in the same location as the assumed target surface location of the measured data's true scene. In contrast, the Wiener filter reconstruction yields an increase in relative distance between the target's front and back surfaces compared to the assumed target location in the original measured data scene. In addition, measuring the squared error or mean squared error of both methods shows a vast improvement of the iterative method over the Wiener filter based on the optimal location of the front and back target surfaces (6th and 10th frames respectively). Based on these reconstruction results, the iterative algorithm is more adequately designed to improve the data's temporal range resolution than the Wiener because it can remove ambiguities in the convolved pulse profiles. The pulse profiles recovered via the iterative algorithm are significantly improved in terms of identifying the surface from which the return pulse reflects. The ability to remove the ambiguity introduced by the width of the pulse on the range estimate suggests additional improvement in range resolution of the LADAR system. Improvement in resolution could potentially exceed the bounds dictated by the actual pulse width of the system.

Deconvolution performance using a Wiener filter varies depending on the value of the noise to signal ratio constant. The optimal Wiener filter was found by varying the constant from values of 1 to 100 and applying the filter to the data. The constant value that provides the sharpest deconvolved profiles is 1/18, the reciprocal number of frames in each data set. The Wiener filter is a poor choice for temporally deconvolving data. Optimal filters providing the sharpest results tend to drive

the maximum and minimum amplitudes further apart and potentially lose total positivity of the data. The smoothing operation performed by the Wiener filter can in some instances degrade data further from the intended result as seen in Figure 4.31, Figure 4.35, and Figure 4.43. This degradation is seen in some of the Wiener filter deconvolved results in Chapter IV. Some of the Wiener filtered pulse profiles experience a decrease in range resolution compared to the convolved data. As a result of the data smoothing, the minimum deconvolved data values may become negative. Data processing can remove the negative values and scale the remaining data to resolve the negativity issue. Another solution to avoid negative values in the deconvolved Wiener filter data is to change the value of the NSR constant. Setting the constant to a value that causes less sharpening in the data can insure positivity of the data. However, this solution decreases the temporal resolution of the resulting deconvolved data. Based on these considerations, the iterative algorithm, again, is the preferred method for temporally deconvolving the data. The iterative algorithm does not contain any parameters that require optimization for improving the temporal resolution of the deconvolved data.

The Wiener filter method does have one advantage over the iterative algorithm. The Wiener filter can deconvolve data much faster than the iterative method. Deconvolving the data sets discussed above with the Wiener filter takes 3.4 seconds. Deconvolving one voxel of data with the iterative algorithm for 10000 iterations takes 20.7 seconds. For 1000 iterations, one voxel for the iterative case takes .24 seconds. Processing each data set (128x128 voxels) using the iterative algorithm for 1000 iterations takes approximately 70 minutes. The Wiener filter is faster but does a poor job deconvolving the target's surface compared to the iterative method. Based on the imaging application, trade offs between algorithm speed and performance for both methods exist and should be considered.

Since the iterative algorithm is derived from the Richardson-Lucy algorithm, analysis of these two algorithms' deconvolution performance seems logical. One reason the Richardson-Lucy algorithm is not included in research testing is the algorithm was derived from data assuming a Poisson

distribution. Real world LADAR data has a negative binomial distribution due to the presence of photon and speckle noise. Therefore, a deconvolution method (Wiener filter) that does not rely on the statistical distribution of the data was chosen for comparison with the iterative algorithm.

5.2 Additional Research

The results from the thesis analysis bring to light several areas of research that should be further examined. More measured data should be taken so a more thorough statistical analysis can be accomplished with the iterative algorithm. With more measured data available, the Cramer-Rao low error bound can be calculated. Cramer-Rao bounds measure an estimator's accuracy. The mean-squared error for any estimate of a non-random parameter has a lower bound, the Cramer-Rao bound, which defines the accuracy of any estimation procedure. Comparisons between the theoretical performance bounds and the actual performance of the measured data sets can be analyzed. A mathematical derivation of the Cramer-Rao bound for the iterative algorithm is attached in Appendix A.

Since the pulse shape and width of the imaging system is unknown, further research could include a blind deconvolution analysis of the measured data using various deconvolution methods including the iterative algorithm. Additional testing would include experimenting with various pulse shapes and widths for each deconvolution method.

One final research area is establishing a decision threshold criteria for detecting and estimating target surfaces to reconstruct a fully deconvolved data set. One possible threshold criteria is the number of photons in a frame of deconvolved data. The decision criteria would allow the researcher to decide if a surface was located in a given frame of data based on the number of photons in the frame.

Appendix A. Derivation of Cramer-Rao Bounds for the Iterative Estimator

Assuming that the estimators for the original non-random profiles are unbiased, the Cramer-Rao bound, or lower bound on the profile estimation error, is determined by calculating the Fisher information matrix. The Fisher information matrix is found by taking the expected value of the second derivative of the log-likelihood function. The derivatives are taken with respect to $o(x, y, k_2)$. Therefore the Fisher matrix can be expressed as

$$J_{ij} = -E[\frac{\delta \ln[f_{D|O}(d|o)]}{\delta o(x, y, k_2)\delta o(x, y, k_3)}]. \tag{A.1}$$

Taking the inverse of this matrix and extracting the diagonal terms yield the Cramer-Rao bounds for the pulse profile estimators. All variance calculations between the profile estimators and the actual profile values should be greater than or equal to the Cramer-Rao bound values. Deriving the Cramer-Rao bound for the profile estimators begins with knowing the log-likelihood function for our parameters of interest. The simplified form of log-likelihood function as mentioned previously is

$$L(o) = \sum_{k=1}^{K} d(x, y, k) \ln\left(i(x, y, k)\right) - \left(d(x, y, k) + M_t\right) \ln\left(i(x, y, k) + M_t\right). \tag{A.2}$$

Differentiating $L(o)$ with respect to $o(x, y, k_2)$ and $o(x, y, k_3)$ yields

$$\frac{\delta L(o)}{\delta o(x, y, k_2)\delta o(x, y, k_3)} = \sum_{k=1}^{K} \frac{d(x, y, k)h(k - k_2)h(k - k_3)}{i(x, y, k)} - \frac{(d(x, y, k) + M_t)h(k - k_2)h(k - k3)}{(i(x, y, k) + M_t)}. \tag{A.3}$$

The expected value of $d(x, y, k)$ is related to the parameters of interest, $o(x, y, k_2)$, via

$$E[d(x, y, k)] = i(x, y, k), \tag{A.4}$$

therefore the Cramer-Rao bound J_{ij}^{-1} simplifies to the following expression

$$J_{ij}^{-1} = \sum_{k=1}^{K} \frac{h(k-k_2)h(k-k_3)M_t}{i(x,y,k)(i(x,y,k)+M_t)}. \tag{A.5}$$

Bibliography

1. Armstrong, Ernest and Stephen C. Cain. "Image Restoration Techniques for Partially Coherent 2-D LADAR Imaging Systems". volume 5562. SPIE Conference on image reconstruction from incomplete data III, July 2004.

2. Cain, Stephen C. "Deconvolution of laser pulse profiles from 3D LADAR temporal returns". volume 5558. SPIE Conference on applications of digital image process XXVII, July 2004.

3. Goodman, J. W. *Statistical Optics*. John Wiley and Sons, 2000.

4. Harsdorf, Stefan and Rainer Reuter. "Stable Deconvolution of Noisy Lidar Signals". pp.88–95. Proceedings of EARSeL-SIG Workshop LIDAR, 2000.

5. Jain, Anil K. *Fundamentals of Digital Image Processing*. Prentice Hall, 1989.

6. Richardson, B.H. "Bayesian-Based Iterative Method of Image Restoration". *J. Opt. Soc. Am.*, 62:pp.55–59, 1972.

7. Schilling, Bradley W., Dallas N. Barr, Glen C. Templeton, Lawrence J. Mizerka, and C. Ward Trussell. "Three-Dimensional Imaging of Obscured Targets by Multiple-Return Laser Radar". Army Science Conference, 2003.

8. Trees, H.L. Van. *Detection, Estimation, and Modulation Theory*. John Wiley and Sons, 1968.

9. Weisstein, Eric W. "Convolution". http://mathworld.wolfram.com/Convolution.html. From MathWorld–A Wolfram Web Resource.

REPORT DOCUMENTATION PAGE

Form Approved
OMB No. 074-0188

1. REPORT DATE *(DD-MM-YYYY)*	2. REPORT TYPE	3. DATES COVERED *(From – To)*
03-21-2005	Master's Thesis	Aug 2003 – Mar 2005

4. TITLE AND SUBTITLE
Deconvolution Analysis of Laser Pulse Profiles from 3-D LADAR Temporal Returns

5a. CONTRACT NUMBER

5b. GRANT NUMBER

5c. PROGRAM ELEMENT NUMBER

6. AUTHOR(S)
Capt. Michael D. Walter

5d. PROJECT NUMBER

5e. TASK NUMBER

5f. WORK UNIT NUMBER

7. PERFORMING ORGANIZATION NAMES(S) AND ADDRESS(S)
Air Force Institute of Technology
Graduate School of Engineering and Management (AFIT/EN)
2950 Hobson Way
WPAFB OH 45433-7765

8. PERFORMING ORGANIZATION REPORT NUMBER
AFIT/GE/ENG/05-22

9. SPONSORING/MONITORING AGENCY NAME(S) AND ADDRESS(ES)
Air Force Research Laboratory
Sensors Directorate, (AFRL/SNJM)
Area B, Bldg 622, "P" St.
WPAFB OH 45433-7765

10. SPONSOR/MONITOR'S ACRONYM(S)

11. SPONSOR/MONITOR'S REPORT NUMBER(S)

12. DISTRIBUTION/AVAILABILITY STATEMENT
Approved for Public Release; Distribution Unlimited

13. SUPPLEMENTARY NOTES

14. ABSTRACT

This work analyzes two deconvolution techniques: Wiener filtering and an iterative process derived from the Richardson-Lucy algorithm. Measured and simulated data are used for testing both methods. 3-D imaging LADAR systems with rapid frame acquisition may lose range resolution due to the transmitted pulse duration. Because of the tradeoff between the need for sufficient target illumination and obtaining high range resolution, LADAR systems often forfeit range resolution performance to improve the signal-to-noise ratio of the observed signal. This work also utilizes these two deconvolution techniques on a sequence of LADAR return images gathered at a very high sampling rate to improve the system's range resolution. Deconvolving the data amplifies any noise present in the data and decreases the signal-to-noise ratio of the reconstructed return pulse profiles. Based on the presence of photon and speckle noise, the work explores the degree to which range resolution can be improved for both measured and simulated data. Squared error and variance calculations are used to evaluate the performance of both signal reconstruction algorithms. The work shows that applying the iterative algorithm to measured and simulated data significantly improves the data's temporal resolution compared to the Wiener filter results.

15. SUBJECT TERMS
3-D laser radar, convolution, temporal resolution, deconvolution, range resolution, image processing, image reconstruction

16. SECURITY CLASSIFICATION OF:			17. LIMITATION OF ABSTRACT	18. NUMBER OF PAGES	19a. NAME OF RESPONSIBLE PERSON
REPORT	ABSTRACT	c. THIS PAGE			Cain, Stephen C., AFIT/ENG
U	U	U		72	19b. TELEPHONE NUMBER *(Include area code)* 937-255-6464 x4408 stephen.cain@afit.edu